

# Characterization of Excited States in Time-Dependent Density Functional Theory Using Localized Molecular Orbitals

Souloke Sen,<sup>1</sup> Bruno Senjean,<sup>2</sup> and Lucas Visscher<sup>1</sup>

<sup>1</sup>*Division of Theoretical Chemistry, Faculty of Sciences, Vrije Universiteit Amsterdam, De Boelelaan 1083, 1081 HV Amsterdam, The Netherlands*

<sup>2</sup>*ICGM, Université de Montpellier, CNRS, ENSCM, Montpellier, France*

(\*Electronic mail: l.visscher@vu.nl)

(Dated: 14 December 2022)

Localized molecular orbitals are often used for the analysis of chemical bonds, but they can also serve to efficiently and comprehensibly compute linear response properties. While conventional canonical molecular orbitals provide an adequate basis for the treatment of excited states, a chemically meaningful identification of the different excited-state processes is difficult within such a delocalized orbital basis. In this work, starting from an initial set of supermolecular canonical molecular orbitals, we provide a simple one-step top-down embedding procedure for generating a set of orbitals which are localized in terms of the supermolecule, but delocalized over each subsystem composing the supermolecule. Using an orbital partitioning scheme based on such sets of localized orbitals, we further present a procedure for the construction of local excitations and charge-transfer states within the linear response framework of time-dependent density functional theory (TDDFT). This procedure provides direct access to approximate diabatic excitation energies and, under the Tamm–Dancoff approximation, also their corresponding electronic couplings – quantities that are of primary importance in modelling energy transfer processes in complex biological systems. Our approach is compared with a recently developed diabatization procedure based on subsystem TDDFT using projection operators, which leads to a similar set of working equations. Although both of these methods differ in the general localization strategies adopted and the type of basis functions (Slater’s vs. Gaussians) employed, an overall decent agreement is obtained.

## I. INTRODUCTION

Time-dependent density functional theory<sup>1–5</sup> (TDDFT) based on the Kohn–Sham<sup>6</sup> (KS) ground-state determinant is a popular method for the calculation of low-lying excited states of medium to large-sized molecules, owing to its favourable accuracy to cost ratio.<sup>4,5,7–9</sup> After the advent of range-separated density functionals that are better suited for describing charge-transfer excitations,<sup>10–17</sup> TDDFT has become the dominant approach for the study of photo-induced processes in biochromophoric systems.<sup>7,18–22</sup> In such processes, excitation energy transfer (EET) and photo-induced electron transfer (ET) pathways play a crucial role.<sup>23,24</sup> A prominent application is found in the study of antenna complexes of photosynthetic systems, responsible for the light-harvesting in higher plants.<sup>25,26</sup> To understand how the initial energy transfer and subsequent charge separation happen, phenomenological models employ a simplified diabatic picture<sup>27–30</sup> such as the Frenkel–Davydov exciton theory, in which the excited-state wavefunction is considered to be a superposition of local excitations (LEs)<sup>31,32</sup> and for which several extensions have been proposed to better describe short-range interactions.<sup>33–38</sup> To connect TDDFT results to these models, it is necessary to express the supermolecular wave function in terms of localized molecular orbitals (LMOs) and to distinguish between LEs and charge-transfer (CT) excitations. Within this local or (approximate) diabatic picture,<sup>39–43</sup> ET and EET processes can be analyzed in a conceptually clear manner.<sup>38,41,42,44,45</sup>

There are two dominant strategies to obtain LMOs and LEs in a supermolecular system.<sup>7</sup> One may either (1) *a priori* partition the supermolecular system into several subsystems and

obtain LMOs from individual calculations on each subsystem, or (2) partition the system *after* a set of supermolecular orbitals is obtained.

The first class of approaches to obtain all relevant supermolecular states in a diabatic picture belongs to the extensive family of embedding techniques.<sup>46–56</sup> In particular, subsystem DFT,<sup>50,57–64</sup> along with its time-dependent extension in the linear response regime, has long been an efficient workhorse for DFT-in-DFT embedding<sup>23,65–69</sup> where different levels of approximations can be used for different subsystems.<sup>70,71</sup> In the second class of approaches, LMOs are obtained by localizing the supermolecular canonical molecular orbitals (CMOs).<sup>72–75</sup> The resulting LMOs can then be used as a starting point for embedding calculations,<sup>76–80</sup> and/or to directly construct (approximate) diabatic states.<sup>45,81–83</sup> As shown by the Neugebauer group, subsystem TDDFT using projection-based embedding techniques can exactly reproduce supermolecular results and capture the complete range of LE/CT interactions.<sup>45,70,79,84,85</sup>

An elaborate discussion of the relations between these two approaches to localization of orbitals and approximate diabatization of electronic states is beyond the scope of this work, and we refer the reader to Refs. 70 and 86 for more details on these methods. To complete this brief list of relevant related methods, we also note the multistate fragmentation excitation difference-fragment charge difference (multistate FED-FCD) method that can also be used to build approximate diabatic states starting from supermolecular CMOs.<sup>44,87–91</sup> By exploiting the spatial locality of LMOs, computationally efficient implementations of TDDFT can be achieved, as shown by Wu and co-workers who demonstrated linear scaling for TDDFT in combination with “fragment

LMOs”.<sup>92</sup> Wu and co-workers also nicely summarized the choices that need to be made in terms of different kinds of locality. Supermolecular CMOs are “local in energy and delocalized in space” while atomic orbitals (AOs) are “local in space but delocalized in energy”. Both types of locality can furthermore be exploited by partially re-canonicalizing the orbital space.<sup>93</sup> Such a partial re-canonicalization step is useful to improve the convergence of the iterative solution of the TDDFT equations as well as for interpretation purposes, as the orbital energies resulting from the re-canonicalization can be readily interpreted as perturbed subsystem energies.

In this work, we build on these previous developments and define a simple and computationally efficient strategy involving a one-step localization procedure to treat LE and CT states. Our approach can be regarded as an extension of our recent work on intrinsic localized fragment (molecular or atomic) orbitals,<sup>94</sup> by adding a re-canonicalization procedure. This step results in a blocked Fock matrix that is similar to the one obtained with the embedding procedure by Tölle *et al.*<sup>45</sup> Since our subsystem orbitals are orthogonal by construction, our procedure does, however, not require the construction of any projection operators.<sup>46,86,95</sup> The procedure allows for a partition of the full orbital space into LE and CT subspaces that are subsequently utilized in a TDDFT calculation to generate approximate diabatic states. Using the Tamm–Dancoff approximation (TDA),<sup>96</sup> explicit expressions for the electronic couplings can be derived between these states. Since our procedure is similar to projection-based subsystem DFT/TDDFT, we compare our result to Ref. 45. Note that the general framework presented here is particularly appealing as it can easily be extended to any excited-state method.

The paper is organized as follows. In the first section, we provide the TDDFT working equations and then outline the construction of the re-canonicalized LMOs, followed by their application as a reference basis in the calculation of excitation energies and electronic couplings in the TDDFT framework. In the next section, a proof of principle application of our method on small model systems is provided, followed by an illustrative example of a chlorophyll dimer in which we also consider the use of additional tight-binding approximations. Conclusions and perspectives are then given in the final section.

## II. THEORY

### A. Time Dependent Density Functional Theory

In the conventional formulation of TDDFT with real spatial orbitals in the adiabatic approximation,<sup>97–99</sup> excitation energies are determined by solving the non-Hermitian eigenvalue problem,

$$\begin{pmatrix} \mathbf{A} & \mathbf{B} \\ -\mathbf{B} & -\mathbf{A} \end{pmatrix} \begin{pmatrix} \mathbf{X} \\ \mathbf{Y} \end{pmatrix} = \omega \begin{pmatrix} \mathbf{X} \\ \mathbf{Y} \end{pmatrix}, \quad (1)$$

where the matrix elements of the  $\mathbf{A}$  and  $\mathbf{B}$  matrices are written as

$$A_{ia,jb} = \delta_{ij}F_{ab} - \delta_{ab}F_{ij} + K_{ia,jb}, \quad (2)$$

and

$$B_{ia,jb} = K_{ia,bj}. \quad (3)$$

In the above equation, indices  $i, j$  denote occupied orbitals and  $a, b$  denote virtual orbitals.  $F_{pq}$  is an element of the KS Fock matrix, and the coupling matrix  $\mathbf{K}$  is defined as

$$K_{ia,jb} = \int d^3\vec{r} \int d^3\vec{r}' \phi_i(\vec{r})\phi_a(\vec{r})f_{\text{Hxc}}[\rho](\vec{r},\vec{r}')\phi_j(\vec{r}')\phi_b(\vec{r}') - c_X \int d^3\vec{r} \int d^3\vec{r}' \phi_i(\vec{r})\phi_j(\vec{r})\frac{1}{|\vec{r}-\vec{r}'|}\phi_a(\vec{r}')\phi_b(\vec{r}'), \quad (4)$$

with the kernel

$$f_{\text{Hxc}}[\rho^{\text{GS}}](\vec{r},\vec{r}') = \frac{1}{|\vec{r}-\vec{r}'|} + (1-c_X)\frac{\delta^2 E_{\text{xc}}[\rho]}{\delta\rho(\vec{r})\delta\rho(\vec{r}')} \Big|_{\rho^{\text{GS}}} \quad (5)$$

consisting of the Coulomb term and the second derivative of the exchange-correlation energy functional  $E_{\text{xc}}[\rho]$ . The second line of (4) allows for use of hybrid DFT approaches that mix in a fraction  $c_X$  of exact exchange.

In the CMO basis, the KS Fock matrix  $F_{pq}^{\text{CMO}} = \delta_{pq}\varepsilon_p$  is diagonal so that different excitation amplitudes  $X_{ia}$  and  $X_{jb}$  are only coupled by the coupling matrix  $\mathbf{K}$ , i.e.,

$$A_{ia,jb}^{\text{CMO}} = \delta_{ij}\delta_{ab}(\varepsilon_a - \varepsilon_i) + K_{ia,jb}, \quad (6)$$

where  $\varepsilon_p$  denotes the energy of orbital  $p$ . The difference between canonical and non-canonical orbitals does not affect the  $\mathbf{B}$  matrix that describes the coupling between excitations and de-excitations. For the sake of simplicity, we will employ the TDA in the following and include excitations only. The equation then reads

$$\mathbf{A}\mathbf{X} = \omega\mathbf{X}, \quad (7)$$

where the lowest eigenvalues and eigenvectors can be obtained by iterative diagonalization techniques. In this work, we first partition the matrix  $\mathbf{A}$  into subsystems to be treated separately.

### B. Construction of Re-canonicalized Intrinsic Localized Molecular Orbitals

In a previous work<sup>94</sup> we introduced the concept of (polarized) intrinsic fragment orbitals (IFOs), a minimal basis in which the supermolecular KS determinant can be expressed exactly. These are constructed from a basis  $B_2$  of reference fragment orbitals (RFOs) that are usually selected as the core and valence orbitals of each fragment. After expressing the supermolecular CMO basis  $B_1$  in terms of these IFOs, both the occupied and virtual valence spaces can be localized to generate a final set of so-called intrinsic localized molecular orbitals (ILMOs), using for instance Pipek–Mezey (PM)

localization.<sup>74</sup> The IFOs and ILMOs span the occupied space exactly but contain only  $N_{B_2} - N_{occ}$  virtual orbitals. Such a truncation of the virtual space is undesirable for the current application to TDDFT, in which we want to retain a sufficient number of virtual orbitals to describe the electronically excited states accurately. A straightforward possibility is to increase the size of the RFO basis ( $N_{B_2}$ ) by selecting more orbitals per fragment, but this will also affect the definition of the valence virtual orbitals that are convenient for interpretation purposes. Another possibility is to keep the minimal valence space as it is, but add a selected number of localized virtual orbitals from the complementary virtual space that is not spanned by the valence virtual orbitals. For this purpose, numerous methods have been developed<sup>100</sup>, which either explicitly rotate these virtual orbitals to increase their localization<sup>73,74</sup> or apply projections of the complementary virtual space onto a predefined set of ‘‘proto-hard’’ atomic virtual orbitals<sup>101</sup>.

In this work, we explore an approach in which the localization of the complementary virtual space that consists of so-called ‘‘hard virtual’’ (hv) orbitals is carried out with the same algorithm as is used for the occupied space. This allows us to work with atomic or molecular fragments, or with a combination of both. Another advantage of our approach is that there is no bias for a particular fragment in defining the initial localization, the procedure can work with an arbitrary number of fragments and allocation of orbitals that are bonding two (or more) fragments together is done after the localization procedure. The key idea is to separate the supermolecular basis into four subspaces:  $B_I = B_{Ic} \cup B_{Im} \cup B_{Iv} \cup B_{Id}$ , with  $B_{Ic}$  indicating core orbitals,  $B_{Im}$  indicating the minimal valence basis (comprising both occupied and virtual orbitals),  $B_{Iv}$  indicating energetically low-lying virtual orbitals, and  $B_{Id}$  indicating energetically high-lying virtual orbitals. The core orbitals in space  $B_{Ic}$  are straightforwardly identified from the orbital energies of the supermolecular calculation and are removed from the orbital set before the localization procedures commences, i.e. we therein use space  $B_I' = B_{Im} \cup B_{Iv} \cup B_{Id}$ . This is a simple extension of our original implementation in which the (usually already very local) core orbitals were also localized. This is now an optional step with as advantage that the core-valence separation is kept exactly as it was in the CMO basis. For the RFOs that comprise reference basis  $B_2$  we similarly partition the relevant part of the orbital space on each fragment as  $B_2 = B_{2m} \cup B_{2v}$ . The procedure is then as follows:

1. Remove core orbitals from  $B_I$  (basis  $B_I'$ ).
2. Define valence RFOs (basis  $B_{2m}$ ).
3. Compute valence IFOs (basis  $B_{Im}$ ).
4. Localize valence orbitals expressed in the IFO basis to obtain valence ILMOs.
5. Define the complementary virtual space  $B_{Iv} \cup B_{Id}$ .
6. Re-canonicalize  $B_{Iv} \cup B_{Id}$  to obtain semicanonical supermolecular virtual orbitals with effective energies  $\epsilon'$ .
7. Select  $N_v$  orbitals with lowest values of  $\epsilon'$  (basis  $B_{Iv}$ ).

8. Define hv RFOs (basis  $B_{2v}$ ).

9. Compute hv IFOs (basis  $B_{Iv}$ ).

10. Localize the hv orbitals expressed in the IFO basis to obtain hv ILMOs.

Steps 2 through 4 are identical to the procedure described in our previous work, reference 94, to which we refer for details about the algorithm and definitions of the valence RFOs, IFOs and ILMOs. Step 5 can also be done before step 4 (as it does not require information about the ILMOs) and is easily implemented by taking the eigenvectors corresponding to the zero eigenvalues of the singular value decomposition (Eq. 15 of reference 94) to define the complementary virtual space  $B_{Iv} \cup B_{Id}$ . Steps 9 and 10 are carried out with exactly the same algorithm as steps 3 and 4 and are implemented by simply changing the arguments to the subroutines that perform these operations. The number of desired virtual orbitals  $N_v$  thereby takes the place of the number  $N_{occ}$  that is used when forming the occupied ILMOs. The advantage of this scheme is that mixing-in of high-energy virtual orbitals into the localized orbital set is strictly prohibited as rotations are only carried out between the lowest  $N_v$  virtual orbitals. In this way we can effectively combine energy selection and orbital localization.

Turning back towards our current application to partitioned TDDFT, we note that all localization transformations are unitary and do not mix the occupied and virtual orbitals that are obtained in the supermolecular calculation. They do therefore not change the structure of the TDDFT (Eq.1) and TDA (Eq.7) equations. The main difference compared to the CMO basis is the appearance of off-diagonal elements in the ILMO basis. In our previous work we observed that the diagonal elements of the transformed Fock matrix can provide an effective energy, but this pragmatic approach is not invariant for rotations that do not affect the localization extent (i.e. rotations between orbitals on the same fragment). It is therefore not well-suited for TDDFT where it is better to have a diagonally dominant  $\mathbf{A}$  matrix. In the current work, we therefore introduce a final re-canonicalization<sup>93</sup> of the occupied and virtual orbitals of each fragment that restores the diagonal dominance and also provides an unambiguous definition of the effective orbital energies. To perform this re-canonicalization, we first sort the ILMO basis such that each orbital is assigned to the fragment on which it has its major contribution, according to Mulliken population analysis.<sup>102</sup> This automatic assignment can optionally be fine-tuned for typical embedding cases in which dangling bonds should always be assigned to the fragment of primary interest. For brevity of notation, we assume from now on a partitioning of the supermolecule into two fragments  $I$  and  $J$ , each with an integer number of occupied and virtual orbitals. After transformation of the supermolecular Fock matrix to this sorted ILMO basis, the subblocks of this Fock matrix, each in a basis of either an occupied or a virtual set of ILMOs, are diagonalized separately as shown in Fig. 1. The resulting eigenvectors form a unitary matrix  $\mathbf{U}^{RILMO}$  that transforms the ILMO basis to the final re-canonicalized ILMO (RILMO) basis. The Fock matrix in RILMO basis is partly di-

agonal,

$$F_{p \in I, q \in I}^{RILMO} = \tilde{\epsilon}_p \delta_{pq}, \quad (8)$$

$$F_{i \in I, a \in J}^{RILMO} = 0, \quad (9)$$

$$F_{i \in I, j \in J \neq I}^{RILMO} \neq 0, \quad (10)$$

$$F_{a \in I, b \in J \neq I}^{RILMO} \neq 0, \quad (11)$$

with  $\tilde{\epsilon}_p$  the eigenvalues obtained in this final re-canonicalization step. These eigenvalues can readily be interpreted as orbital energies of the fragments, perturbed by the interaction with the other fragment(s). By choosing chemically relevant fragments, it is possible to identify  $\pi$  and  $\pi^*$  orbitals of conjugated aromatic systems that are delocalized over a single fragment only.

Given the similarity in structure of the Fock matrix in the RILMO basis with those arising in projection-based embedding, our re-canonicalization procedure can be seen as a one-step embedding where the resulting RILMOs are comparable to a set of polarized orthonormal subsystem orbitals re-

sulting from a top-down embedding scheme.<sup>45,54,79,84–86</sup> The main advantage of the current procedure is its simplicity and efficiency: the generation of ILMOs is done via an iterative Jacobi algorithm that typically shows a rapid convergence, whereas the diagonalizations needed for the re-canonicalizations are done in subspaces of the full CMO space. The whole procedure therefore takes only a fraction of the time needed for the supermolecular DFT calculation and is carried out by a dedicated program requiring only the definition of the supermolecular and fragment orbitals and the atomic basis in which these are expressed.

Within the RILMO basis, characterization of LE and CT excitations for TDDFT calculations is easy. Choosing again two subsystems, 1 and 2, and labeling the excitations as either local ( $L_1$  and  $L_2$ ) or as electron transfer from system 1 to 2 ( $CT_1$ ) or vice versa ( $CT_2$ ) we obtain the same structure for the TDA equation (7) as found in projection-based embedding<sup>45,54,79,84</sup>, but without explicit use of projectors.

$$\begin{pmatrix} \mathbf{A}^{L_1} & \mathbf{A}^{L_1/L_2} & \mathbf{A}^{L_1/CT_1} & \mathbf{A}^{L_1/CT_2} \\ \mathbf{A}^{L_2/L_1} & \mathbf{A}^{L_2} & \mathbf{A}^{L_2/CT_1} & \mathbf{A}^{L_2/CT_2} \\ \mathbf{A}^{CT_1/L_1} & \mathbf{A}^{CT_1/L_2} & \mathbf{A}^{CT_1} & \mathbf{A}^{CT_1/CT_2} \\ \mathbf{A}^{CT_2/L_1} & \mathbf{A}^{CT_2/L_2} & \mathbf{A}^{CT_2/CT_1} & \mathbf{A}^{CT_2} \end{pmatrix} \begin{pmatrix} \mathbf{X}^{L_1} \\ \mathbf{X}^{L_2} \\ \mathbf{X}^{CT_1} \\ \mathbf{X}^{CT_2} \end{pmatrix} = \omega \begin{pmatrix} \mathbf{X}^{L_1} \\ \mathbf{X}^{L_2} \\ \mathbf{X}^{CT_1} \\ \mathbf{X}^{CT_2} \end{pmatrix}, \quad (12)$$

We can now identify couplings between local and charge-transfer excitations as off-diagonal blocks of the  $\mathbf{A}$  matrix.<sup>79,86</sup> Thanks to the re-canonicalization and equation (8), the diagonal blocks have the same structure as in the CMO basis, i.e. Eq. (6). For the off-diagonal blocks, we need to employ the more general expression (2) to account for Eqs. (10) and (11). Without truncation the results in the RILMO basis will be identical to those obtained in the CMO basis as we will numerically verify in section IV A. Obviously, this case is not of practical interest, as one aims to reduce the computational cost of the method. Hence, we consider two subsequent truncations that will each affect the results: (i) reduction of the size of the RILMO basis by limiting the total number of virtual orbitals  $N_V$  that are localized and (ii) reduction of the number of couplings between subsystems that are accounted for by restricting the solution of the TDA equation to only one or a few subsets of excitations. In the following, we refer to applying (ii) as the ‘reduced diagonalization’ (RD), as opposed to the ‘complete diagonalization’ (CD) when (ii) is not applied. One should keep in mind that the truncation (i) can be so severe that even the CD results will significantly deviate from the full CMO treatment. We will therefore first study the effect of this initial truncation (i), referred to as the ‘‘RILMO truncation’’.

### C. Reduced diagonalization

As the number of solutions sought is typically far smaller than the dimension of the  $\mathbf{A}$  matrix, it is advantageous to use a Davidson diagonalization algorithm.<sup>103</sup> We can thereby make use of the partitioning, and solve each particular subset  $S$  of excitations individually, initially without accounting for couplings between the subsets,

$$\mathbf{A}^S \mathbf{V}^S = \omega^S \mathbf{V}^S. \quad (13)$$

For a partitioning into two subsystems, the eigenvectors  $\mathbf{V}_\gamma^S$  associated with the excitation energies  $\omega_\gamma^S$  can be interpreted as approximate diabatic states corresponding to  $L_1$ ,  $L_2$ ,  $CT_1$  and  $CT_2$ . They are subsequently coupled to form adiabatic states via

$$\bar{\mathbf{A}} \bar{\mathbf{W}} = \bar{\omega} \bar{\mathbf{W}}, \quad (14)$$

with the matrix elements of  $\bar{\mathbf{A}}$  defined as

$$\bar{A}_{\gamma\delta}^S = \delta_{\gamma\delta} \omega_\gamma^S \quad (15)$$

$$\bar{A}_{\gamma\delta}^{S/T} = \sum_{ia \in S} \sum_{jb \in T} V_{ia,\gamma}^S A_{ia,jb}^{S/T} V_{jb,\delta}^T, \quad (16)$$

yielding the coefficient vector  $\bar{\mathbf{W}}$  which expresses the adiabatic state in terms of the diabatic states. This approach can be generalized to many subsystems, with the efficiency arising

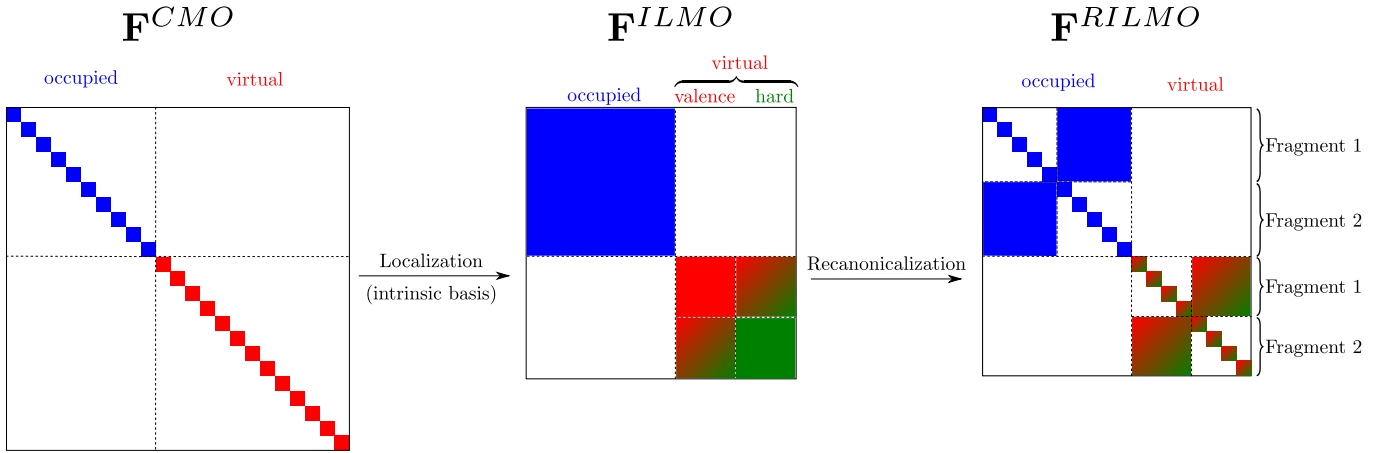


FIG. 1: Representation of the Fock matrix in different bases. Colored blocks represent non-zero matrix elements, where the smaller squares are single matrix elements.

from the fact that only a small number  $M^S$  of lowest eigenvectors for each excitation subset  $S$  is used. The resulting  $M = \sum_S M^S$  dimensional matrix problem for the full system is then easily solvable. The calculation of the electronic couplings between subsystems and subsequent diagonalization in a reduced space has a similar structure as encountered in the subsystem TDA approach, as discussed in Refs. 67 and 45. Hence, RD consists in constructing and subsequently diagonalizing (see Eq. 14) a basis of approximate diabatic states, where only a limited set of the lowest diabatic states per subspace is considered. The RD pathway for a case of two subsystems is schematically depicted in Fig. 2 and can be summarized as:

1. Starting from the set of RILMOs, partition the occupied and virtual orbitals and perform four separate TDA calculations to obtain sets of eigenvectors  $\{\mathbf{V}_\gamma^S\}$  for each of the  $L_1$ ,  $L_2$ ,  $CT_1$  and  $CT_2$  sub-spaces.
2. Calculate electronic couplings between the diabatic states using the sets of eigenvectors from the previous step and construct matrix  $\bar{\mathbf{A}}$ ,
3. Diagonalize  $\bar{\mathbf{A}}$  to obtain the adiabatic states.

Note that in the limit of including all the diabatic states for each subspace, the CD and RD procedures yield identical results.

#### D. Evaluation of the coupling elements

The most time-consuming steps in the calculation are the matrix-vector multiplications, in which trial vectors are contracted with a block of the  $\mathbf{A}$  matrix. We will briefly summarize our implementation, which is based on the pair-fitting approach of the ADF engine of the Amsterdam Modelling Suite (AMS), as described in Ref. 5. We first define the RILMOs in terms of atomic orbitals  $\chi$  as

$$\phi_l(\mathbf{r}) = \sum_{\kappa} C_{\kappa l}^{RILMO} \chi_{\kappa}(\mathbf{r}), \quad (17)$$

and introduce the density functions  $f_p$  to fit the transition densities  $\rho_{\delta}^T(\mathbf{r})$  of state  $\delta$  of subspace  $T$

$$\rho_{\delta}^T(\mathbf{r}) = \sum_{jb \in T} \phi_j(\mathbf{r}) \phi_b(\mathbf{r}) V_{jb, \delta}^T \approx \sum_p f_p(\mathbf{r}) c_{p\delta}^T. \quad (18)$$

The fit coefficients  $c_{p\delta}^T$  can be expressed in terms of atomic orbital fit coefficients  $\mathbf{c}^{AOfit}$  and the (trial)  $\mathbf{V}$  matrices as

$$c_{p\delta}^T = \sum_{jb \in T} \sum_{\kappa, \lambda} C_{\kappa j}^{RILMO} C_{\lambda b}^{RILMO} c_{\kappa \lambda, p}^{AOfit} V_{jb, \delta}^T. \quad (19)$$

Using Eq. (18), the induced potential  $\delta v_{ind, \delta}^T$  for state  $\delta$  of subspace  $T$  can then be written as

$$\delta v_{ind, \delta}^T(\mathbf{r}) = \sum_p [g_p(\mathbf{r}) + f_{xc}(\mathbf{r}) f_p(\mathbf{r})] c_{p\delta}^T, \quad (20)$$

with  $g_p(\mathbf{r})$  the Coulomb potential of the fit function  $f_p(\mathbf{r})$  and  $f_{xc}(\mathbf{r})$  the exchange-correlation kernel. The matrix representation of the induced potential in the RILMO excitation basis of subspace  $S$  can subsequently be obtained by numerical integration

$$[\delta v_{ind, \delta}^T]_{ia}^S = \sum_k w_k \phi_i(\mathbf{r}_k) \delta v_{ind, \delta}^T(\mathbf{r}_k) \phi_a(\mathbf{r}_k), \quad (21)$$

with  $w_k$  the weight associated to the grid point  $\mathbf{r}_k$ . Because the functions  $\phi_i$  and  $\phi_a$  are local, detection and neglect of small contributions to the integrand can be used to speed up this step.

For hybrid functionals, we also need to consider the exchange contribution. Here, density fitting can be used as well, using the implementations reported in Refs. 104 and 105. The exchange contribution to the induced potential is given by

$$[\delta v_{exc, \delta}^T]_{ia}^S = \sum_{jb \in T} (ij|ab) V_{jb, \delta}^T, \quad (22)$$

which is first expressed in the AO basis and evaluated using

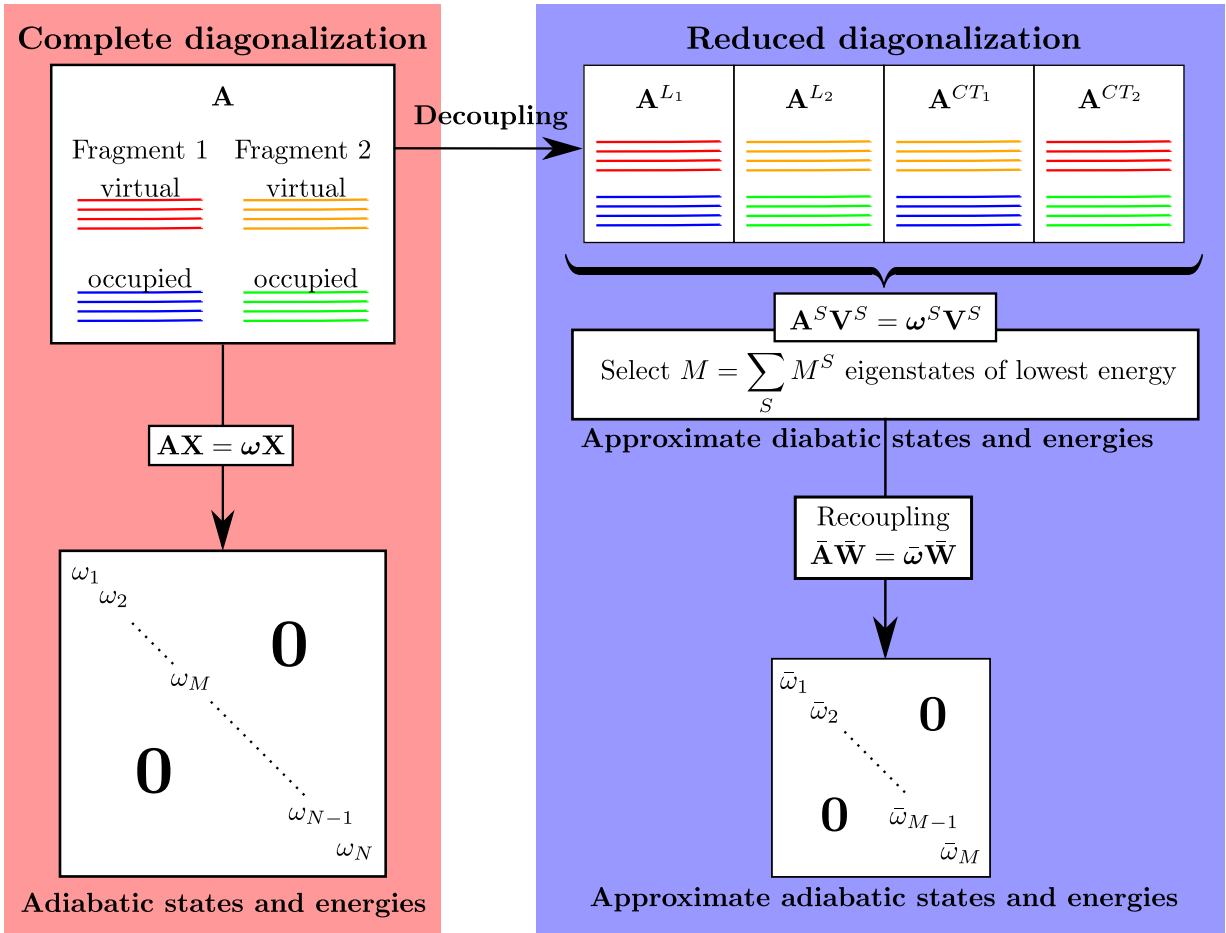


FIG. 2: RD procedure for obtaining the LE and CT states and electronic couplings using RILMOs.

density fitting as

$$[\delta v_{exc,\delta}^T]_{\kappa\lambda} = \sum_{\mu\nu} (\kappa\mu|\lambda\nu) V_{\mu\nu,\delta}^T \approx \sum_{\mu\nu} \sum_{p,q} c_{\kappa\mu,p}^{AOfit} c_{\lambda\nu,q}^{AOfit} (f_p|f_q) V_{\mu\nu,\delta}^T, \quad (23)$$

with

$$V_{\mu\nu,\delta}^T = \sum_{jb \in T} C_{\mu j}^{RILMO} C_{\nu b}^{RILMO} V_{jb,\delta}^T. \quad (24)$$

After a transformation to the excitation subspace  $S$

$$[\delta v_{exc,\delta}^T]_{ia}^S = \sum_{\kappa\lambda} C_{\kappa i}^{RILMO} C_{\lambda a}^{RILMO} [\delta v_{exc,\delta}^T]_{\kappa\lambda}, \quad (25)$$

this term can be combined with the other contributions. The total electronic coupling in Eq. (16) between two excitations  $\gamma$  and  $\delta$  belonging to the  $S$  and  $T$  subspaces then becomes

$$\begin{aligned} \bar{A}_{\gamma\delta}^{S/T} &= \sum_{ia \in S} \sum_{jb \in T} V_{ia,\gamma}^S (F_{ij}^{RILMO} \delta_{ab} - F_{ab}^{RILMO} \delta_{ij}) V_{jb,\delta}^T \\ &+ \sum_{ia \in S} V_{ia,\gamma}^S \left( [\delta v_{ind,\delta}^T]_{ia}^S - c_x [\delta v_{exc,\delta}^T]_{ia}^S \right). \end{aligned} \quad (26)$$

### E. Tight-binding approximations to the coupling matrix

The above-mentioned scheme can also be easily applied to approximate TDDFT approaches. An example is Grimme's simplified TDA<sup>106</sup> in which matrix elements of the coupling matrix  $\mathbf{K}$  are given as

$$K_{ia,jb} = \sum_{A,B}^{N_{atoms}} (2q_{ia}^A \gamma_{AB}^J q_{jb}^B - q_{ij}^A \gamma_{AB}^K q_{ab}^B), \quad (27)$$

with atomic transition charges  $q_{pq}^A$  obtained as

$$q_{pq}^A = \sum_{\mu \in A} C'_{\mu p} C'_{\mu q}. \quad (28)$$

The parameters  $\gamma_{AB}^J$  and  $\gamma_{AB}^K$  depend on the interatomic distance and the chemical hardness of the atoms as well as on a few empirical parameters. The matrix  $\mathbf{C}'$  denotes MO coefficients in the orthogonal AO basis obtained from  $\mathbf{C}' = \mathbf{S}^{1/2} \mathbf{C}$  with  $\mathbf{C}$  the coefficients in the original AO basis and  $\mathbf{S}$  the AO overlap matrix. This approach is easily adapted to the RILMO partitioning by just replacing the CMOs by the RILMOs in Eqs. (27) and (28).

### III. COMPUTATIONAL DETAILS

All DFT and TDDFT calculations using the RILMOs were carried out using a locally modified version of the Amsterdam Modelling Suite of Programs<sup>107,108</sup> (AMS). For all TDDFT calculations in AMS, the ALDA kernel and TDA were used throughout this work (denoted as RILMO-TDA). The localization and re-canonicalization of the molecular orbitals were carried out separately using a recently developed stand-alone program, so-called Reduction of Orbital Space Extent (ROSE) that has an interface to AMS<sup>94,109</sup>. All calculations for ROSE and AMS were automated using the Python Library for Automating Molecular Simulation<sup>110</sup> (PLAMS) of AMS. The sorting of the orbitals before the re-canonicalization step was done based on a Mulliken population analysis of the LMOs over each fragment. In this work we used the same level of basis sets,  $\mathcal{B}_1$  and  $\mathcal{B}^k$ , for the supermolecule and the  $k$  fragments respectively (see reference 94 for the notations). For the localization step, we used the Pipek–Mezey localization for both the occupied and the virtual orbitals.<sup>74</sup> For TDDFT calculations with the Grimme’s simplified Tamm–Dancoff<sup>106</sup> approximation (denoted as RILMO-simTDA), the parameters from Ref. 106, corresponding to the standard settings in AMS, were used.

All projection-based embedding subsystem DFT (PbE-sDFT) and TDDFT/TDA calculations (denoted as PbE-sTDA) calculations were carried out using SERENITY version 1.4.0<sup>111</sup> with the LevelShift projection<sup>112</sup> operator of the top-down embedding<sup>79,85,86</sup> procedure as outlined in Ref. 86. Additional localization of the virtual orbitals was carried out using the approach outlined in Ref. 85 as implemented inside SERENITY. In all the calculations performed in SERENITY, the resolution of identity (RI)<sup>113</sup> approximation was used for the evaluation of the Coulomb contribution in all the DFT and TDDFT/TDA<sup>114</sup> calculations.

### IV. RESULTS AND DISCUSSIONS

#### A. RILMO truncation and Complete versus Reduced Diagonalization

In order to demonstrate our procedure, we choose two test systems: the ethylene-tetrafluoroethylene dimer and the adenine-thymine DNA base pair. While the former presents an adequate model for studying LE and CT type transitions, the latter provides a biologically relevant model system where such quantities are of importance to model the stability of biomolecules under irradiation<sup>115,116</sup>. The geometry of both of these structures were taken from Ref. 45 and Ref. 115 and is displayed in Fig. 3a and 3b, respectively. The CAM-B3LYP<sup>13</sup> exchange-correlation functional along with the Slater-type basis set TZ2P as employed in AMS was used for both these systems.

The uncoupled LE (uLE) and uncoupled CT (uCT) states considered for both systems consist of  $\pi \rightarrow \pi^*$  type transitions. Fig. 4 (middle column) and Fig. 5 (middle row) plot the

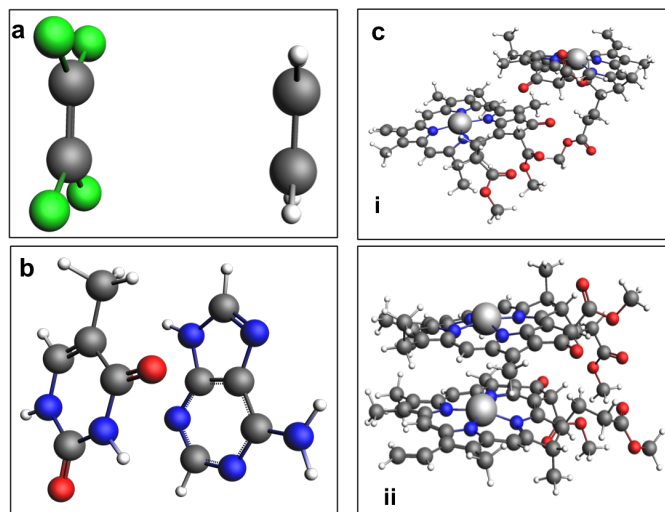


FIG. 3: Geometries of the a) tetrafluoroethylene-ethylene dimer, b) adenine-thymine base pair, and c) chlorophyll dimer.

relevant  $\pi$  and  $\pi^*$  RILMOs associated with the  $C_2H_4 - C_2F_4$  dimer and the adenine-thymine dimer, respectively. The corresponding supermolecular CMOs are also shown. The CMOs are delocalized over both fragments, and the localization and re-canonicalization procedures restore the typical  $\pi$  and  $\pi^*$  character in the RILMOs. For comparison, we show the PbE-sDFT orbitals that yield a similar localized picture.

For the ethylene-tetrafluoroethylene dimer we consider two uLE states for  $C_2H_4$ , one uLE for  $C_2F_4$  and one uCT state from  $C_2F_4 \rightarrow C_2H_4$ . For  $C_2H_4$  we have a  $\pi \rightarrow \pi^*$  state and a  $\pi \rightarrow \sigma^*$  state which is near-degenerate with the former. These two states mix upon increasing the size of the virtual space in the localization procedure, so that we will denote them as uLE<sub>1</sub> and uLE'<sub>1</sub> below. In the limit of the full virtual space, the uLE<sub>1</sub> retains mostly the  $\pi \rightarrow \pi^*$  character ( $\sim 71\%$ ). For  $C_2F_4$  we have a  $\pi \rightarrow \pi^*$  state denoted as uLE<sub>2</sub> and for the CT transition we have a  $C_2F_4, \pi \rightarrow C_2H_4, \pi^*$  state denoted as uCT. For the adenine-thymine dimer, we label the two near-degenerate adenine  $\pi \rightarrow \pi^*$  states (originally denoted  $L_a$  and  $L_b$  in Ref. 115) as uLE<sub>1a</sub> and uLE<sub>1b</sub>, while denoting the thymine  $\pi \rightarrow \pi^*$  state as uLE<sub>2</sub>. Besides these three uLE states, there is one uCT state: adenine,  $\pi \rightarrow$  thymine,  $\pi^*$ . It is important to note that the above set of four excitations for both of these dimers does not constitute the lowest set of excitations but selects the primary valence  $\pi \rightarrow \pi^*$  type transitions that are often used to model LE and CT type excitations in the literature.

As a numerical verification of our implementation, we first show that the supermolecular excitation spectrum arising from the CD (see Fig. 2) of RILMO-TDA converges to the CMO results in the limit of using the full virtual space. Fig. 6 plots the error in the energy of the lowest RILMO-TDA states from the CMOs as a function of the virtual space size, i.e from severe to no RILMO truncation. Besides the expected convergence, the plot also indicates that RILMO truncation is a viable way to restrict the excitation space. A modest amount of virtual

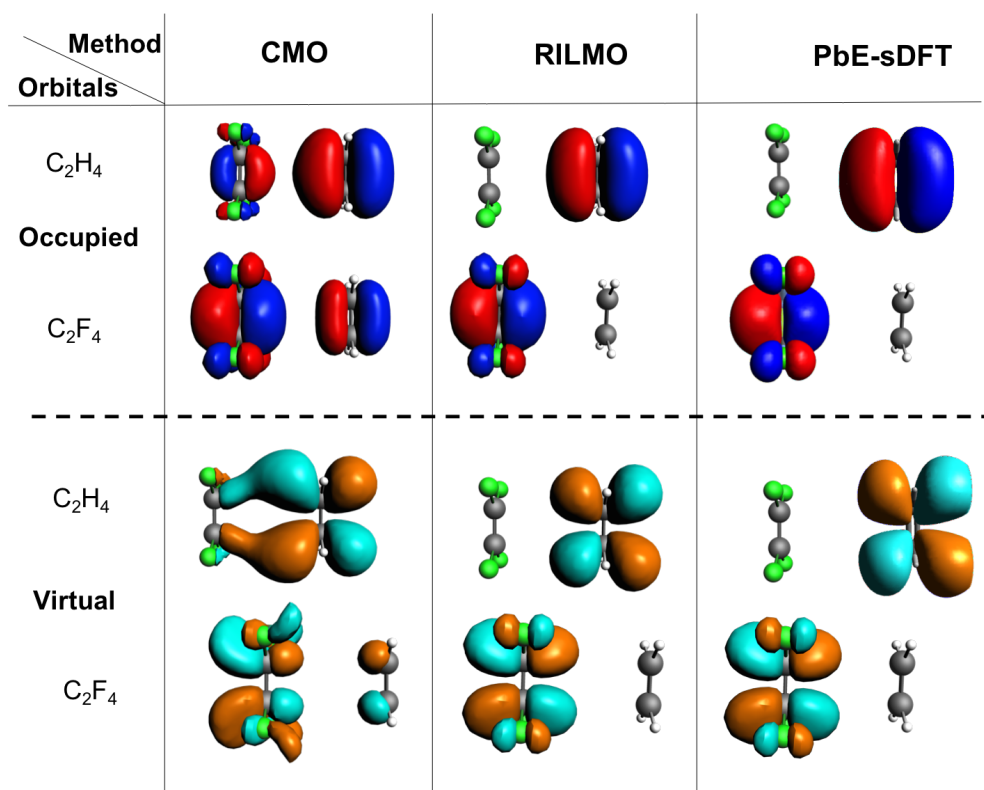


FIG. 4: The occupied and virtual orbitals associated with the uLE and uCT states for the  $C_2H_4 - C_2F_4$  dimer obtained from CMOs (left column), RILMOs (middle column) and PbE-sDFT (right column).

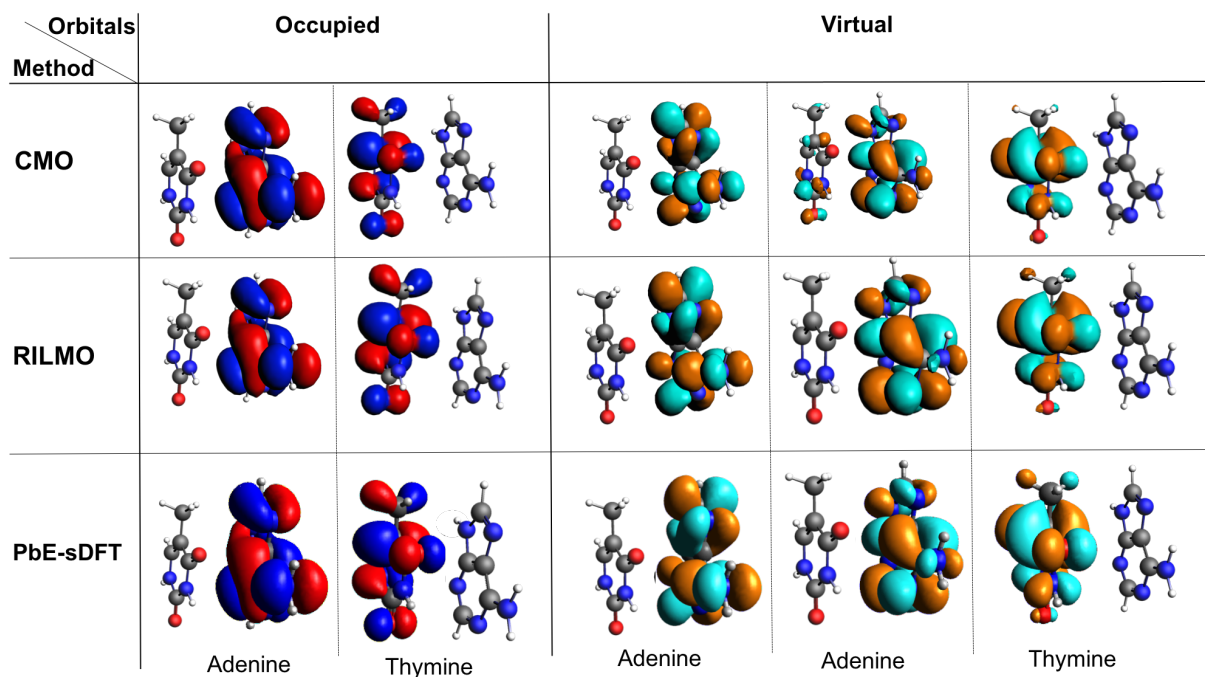


FIG. 5: The occupied and virtual orbitals associated with the uLE and uCT states for the adenine-thymine dimer obtained from CMOs (top row), RILMOs (middle row) and PbE-sDFT (bottom row).

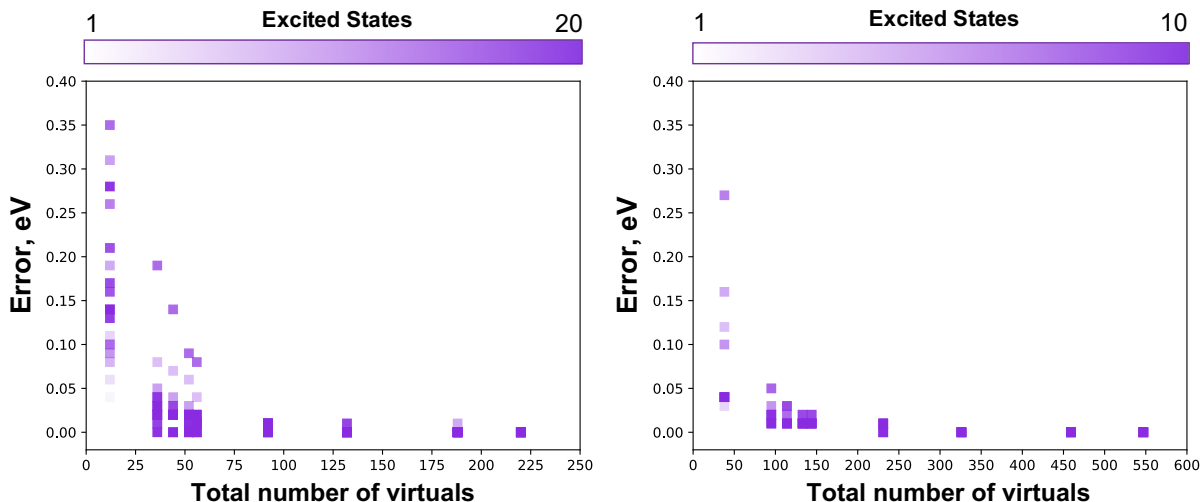


FIG. 6: Error in excitation energy (as compared to the supermolecular CMO reference energies) due to RILMO truncation of hv orbitals. Left panels: lowest 20 RILMO-TDA (CD) states for the  $C_2H_4 - C_2F_4$  dimer. Right panels: lowest 10 RILMO-TDA (CD) states of the adenine-thymine dimer.  $M$  denotes the number of diabatic states (top panels:  $M = 20$ , bottom panels:  $M = 80$ ). The color of the marker indicates the energy ordering of states.

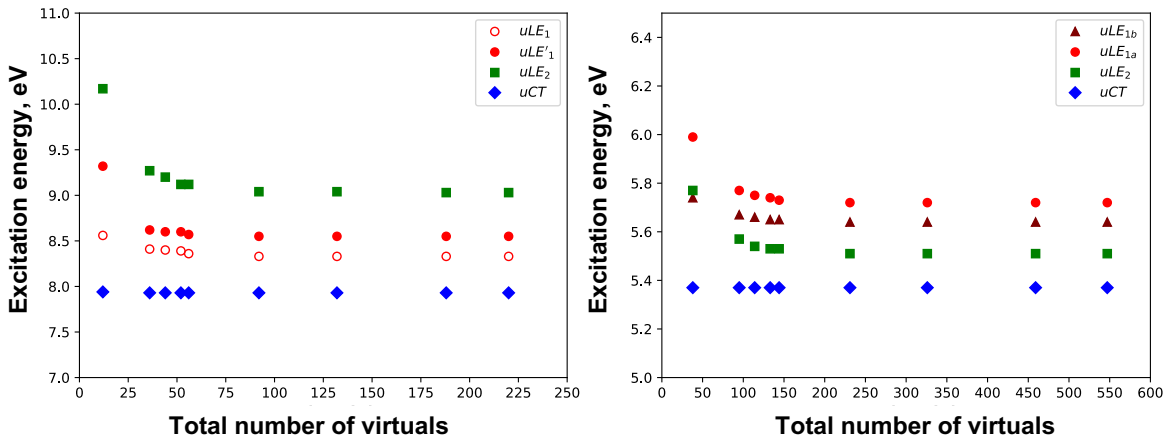


FIG. 7: Left panel: Excitation energy of the uLE and uCT states using RILMO-TDA (RD) for the  $C_2H_4 - C_2F_4$  dimer with respect to the number of hv orbitals used in the localization procedure. Right panel: same as the left panel for the adenine-thymine dimer.

orbitals suffices to obtain adiabatic state energies close to the reference supermolecular CMO results.

Next, we consider combining RILMO truncation with truncation in the number of diabatic states employed in the RD scheme. For this purpose, we couple for both dimers only the aforementioned sets of four uLE and uCT states. Fig. 7 shows the effect of RILMO truncation combined with RD. From Fig. 7, we observe a decrease in the uLE energies for both the  $C_2H_4 - C_2F_4$  and adenine-thymine dimers, whereas the uCT energies are quite stable upon increasing the number of virtual orbitals. This stability can be explained by the fact that the CT excitations are well described by single orbital transitions,<sup>117</sup> so that moving from a minimal valence

space to the full virtual space causes little to no change in the corresponding excitation energies. The LE excitations, on the other hand, are mixtures of local single orbital transitions and are thus more sensitive to the number of virtual orbitals. The uLE excitation energies exhibit a smooth convergence upon increasing the number of virtual orbitals, similar to what is seen for isolated or well-separated fragments (see SI, Figs. S1 and S2).

Fig. 8 plots the corresponding coupled adiabatic states using the above four diabatic states for both of these dimers. As can be seen, the curves follow closely the uncoupled energies and converge smoothly upon increasing the total number of virtual orbitals. Figs. 7 and 8 show that it is sufficient to work

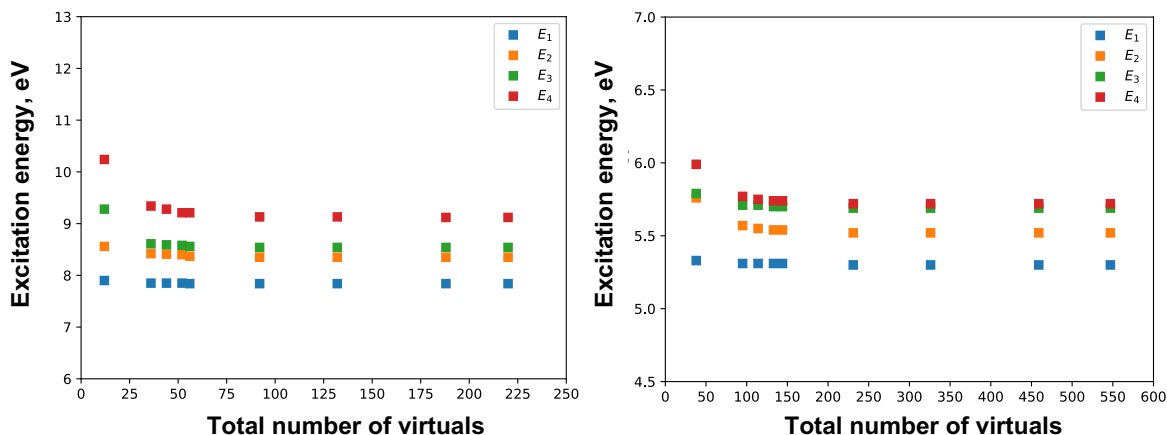


FIG. 8: Excitation energies of the coupled states using the minimal set of four diabatic states for the  $C_2H_4 - C_2F_4$  (left panel) and adenine-thymine (right panel) dimers with respect to the number of hv orbitals used in the localization procedure.

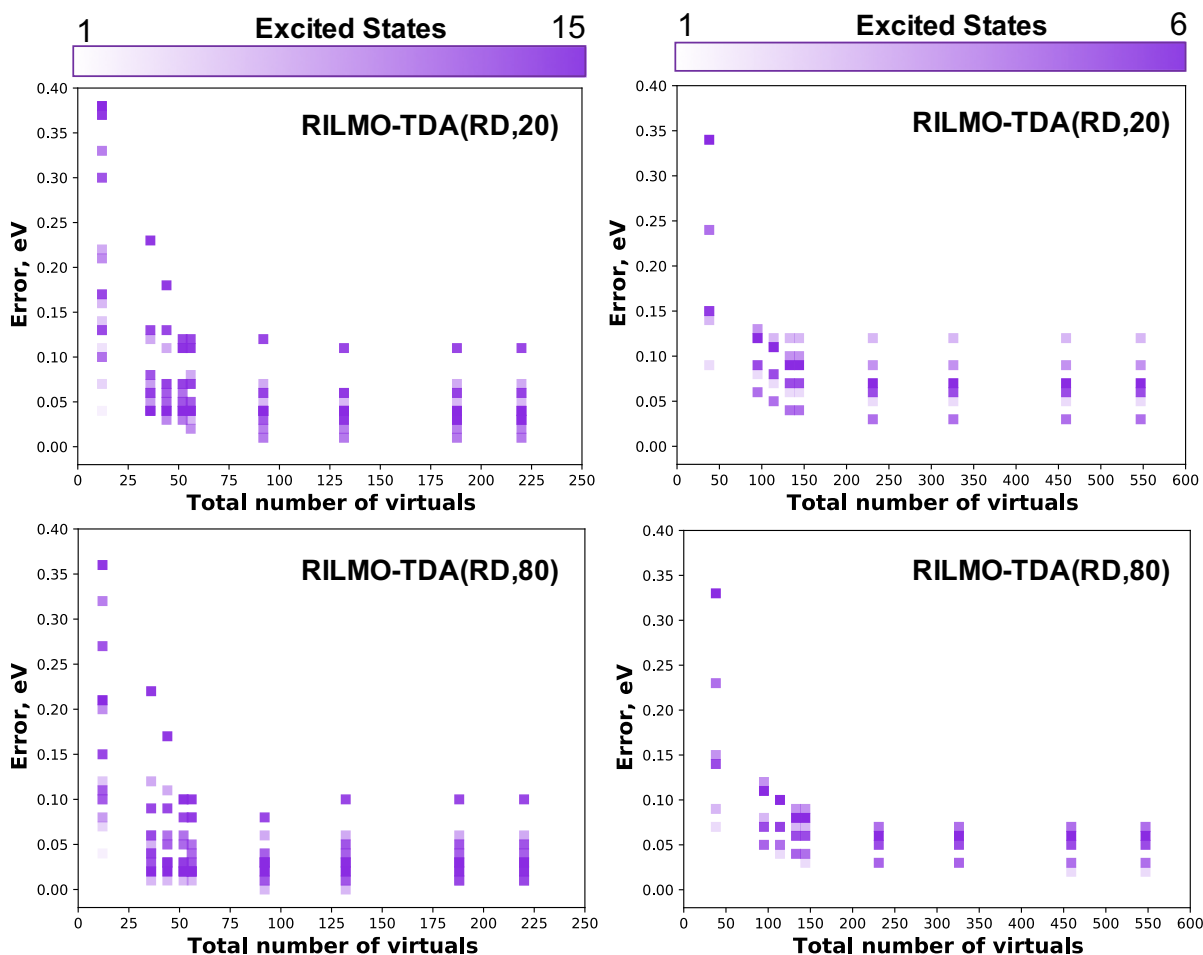


FIG. 9: Error in excitation energy (as compared to the supermolecular CMO reference energies) due to RILMO truncation of hv orbitals. Left panels: lowest 15 RILMO-TDA (RD, $M$ ) states for the  $C_2H_4 - C_2F_4$  dimer. Right panels: lowest 6 RILMO-TDA (RD, $M$ ) states of the adenine-thymine dimer.  $M$  denotes the number of diabatic states (top panels:  $M = 20$ , bottom panels:  $M = 80$ ). The color of the marker indicates the energy ordering of states.

with a modest number of virtual orbitals to construct the local states in the RD framework.

Having thus shown that RILMO truncation in combination with RD is viable, we also consider the RD procedure itself in more detail. To do so, we couple the above minimal set of four diabatic states with additional low-lying states and investigate how this changes the excitation energies. Fig. 9 plots the error in the excitation energies of the lowest RILMO-TDA adiabatic states from their respective CMO states. We thereby chose a simple set up, taking either the lowest 5 or the lowest 20 diabatic states in each of the four excitation subspaces, yielding a total of 20 and 80 adiabatic states, respectively. A direct comparison of all resulting states with CMO states is complicated, as the coupling of adiabatic states also gives rise to high-energy states that can not be readily matched with CMO states. For this reason, we focus on the lowest energy states up to the above-mentioned bright  $\pi \rightarrow \pi^*$  excitations. As can be seen for both of these dimers, increasing the total number of states from 20 to 80 shows a reduction in the overall deviation of the lower-lying states to well within one-tenth of an eV, again already with a modest amount of virtual orbitals (i.e. with strong RILMO truncation). From Fig. 9, we conclude that for the  $C_2H_4 - C_2F_4$  and adenine-thymine dimers, a set of five states for each of the subspaces is sufficient to closely reproduce the lowest CMO states, including the characteristic  $\pi \rightarrow \pi^*$  transitions. As an additional proof of principle, we have further checked the smooth convergence of the lowest 10 RILMO-TDA adiabatic states towards the reference supermolecular CMO states, with respect to the  $M$  number of diabatic states used in the RD pathway on a smaller water-ammonia test system (see Fig. S4 in SI).

## B. Comparison with projection-based embedding subsystem DFT

Having shown the convergence towards the supermolecular CMO results for the CD and RD pathways, we now focus on a more detailed comparison of the above approximate diabatic uLE and uCT states as well as their electronic couplings with those obtained from PbE-sDFT/sTDA. For the sake of consistency, we retain the full virtual space in the RILMO-TDA calculation of the above dimers. Both of these systems have been studied in Ref. 45 and their diabatic LE and CT states were obtained using the multistate-FCD-FED approach and PbE-sTDA by employing different orbital partition schemes for varying displacements  $\mathbf{d}$  between the corresponding monomers. In Ref. 45, an overall decent agreement was obtained between the two methods in spite of their differences in the construction of the diabatic states. We refer the reader to Ref. 45 for more details, and only the necessary PbE-sDFT/sTDA calculations are repeated here for comparison. For the purpose of this work, the Gaussian type def2-TZVP basis set was chosen in SERENITY in order to compare with the Slater-type basis set TZ2P as employed in AMS. While the two basis sets are reasonably large, the effect of basis set truncation is still nonnegligible as can be seen when comparing the supermolecular CMO results of the two codes.

In Fig. 10 (top panel) we plot the differences in the lowest 10 excitation energies and see that these can amount to a few tenths of eV, with the most pronounced differences occurring for the  $C_2H_4 - C_2F_4$  dimer. While for the Adenine-Thymine dimer our states of interest (the characteristic  $\pi \rightarrow \pi^*$  transitions) lies within the lowest 6 supermolecular CMO states (states 2,3,5 and 6), such an identification for the  $C_2H_4 - C_2F_4$  dimer becomes difficult due to the delocalized nature of the CMOs as shown in Fig. 4.

To compare the ground-state embedded orbitals, we again refer to Fig. 4 (right column) and Fig. 5 (bottom row) for the relevant  $\pi$  and  $\pi^*$  orbitals of  $C_2H_4 - C_2F_4$  and the adenine-thymine dimer. We see that despite differences in the formalism, and type of basis functions employed, both embedding procedures lead to very similar local orbitals for both systems.

Focusing first on the lowest uCT state in each dimer, Fig. 11 plots the uCT energy from RILMO-TDA along with the corresponding uCT energy from PbE-sTDA as a function of the separation distance between the monomers. Both methods agree very well at longer distances, displaying the asymptotic decay of  $-R^{-1}$  characteristic for CT states. At shorter distances, the uLE energies from RILMO-TDA are consistently lower compared to those of PbE-sTDA (see Table I for uLE<sub>1</sub>, Table S1 in SI for the energies of uLE<sub>1</sub><sup>'</sup>, and Table II). Besides the already mentioned difference in basis sets, the deviation observed between the uCT energies could also arise from the differences in the two methods, in particular the different localization of the virtual orbitals. In the PbE approach, the virtual orbitals are subject to a SVD of the MO overlap matrix computed with only the AO basis functions located on the fragment of interest to obtain virtual LMOs for that fragment<sup>45,85</sup>. In our scheme, on the other hand, the virtual orbitals are subject to two separate PM localizations, resulting in a small set of ‘valence’ virtual orbitals and a larger set of ‘hard’ virtual orbitals. The resulting differences in virtual orbital energies, which in the PbE case rise more steeply upon reducing the monomer distance, appear to be the main cause for this difference (see Tables S2 and S3 in SI).

The differences observed at short distances and agreements at long distances are also reflected in the electronic couplings between the respective uLE and uCT states. Fig. 12 plots their absolute values as a function of the separation distance between the monomers for each of these dimers. Only a few illustrative couplings are shown, see Fig. S5 and S6 in SI for all the couplings. The couplings between the uLE and uCT states calculated from both of the two methods display an exponential decay ( $e^{-r}$ ) at long range, which is typical for exchange interactions. The most significant difference between the methods is seen in the uLE<sub>1</sub>/uCT coupling of the  $C_2H_4 - C_2F_4$  dimer, where the coupling is stronger for PbE-sTDA at short distances and weaker at long distances, as compared to RILMO-TDA. For the other couplings, the two methods give qualitatively similar results.

As both the PbE-sTDA and our approach converge to the supermolecular CMO results when sufficient states are coupled, we also show in Fig. 10 (bottom panel), the excitation energies obtained when a total of 80 diabatic states are cou-

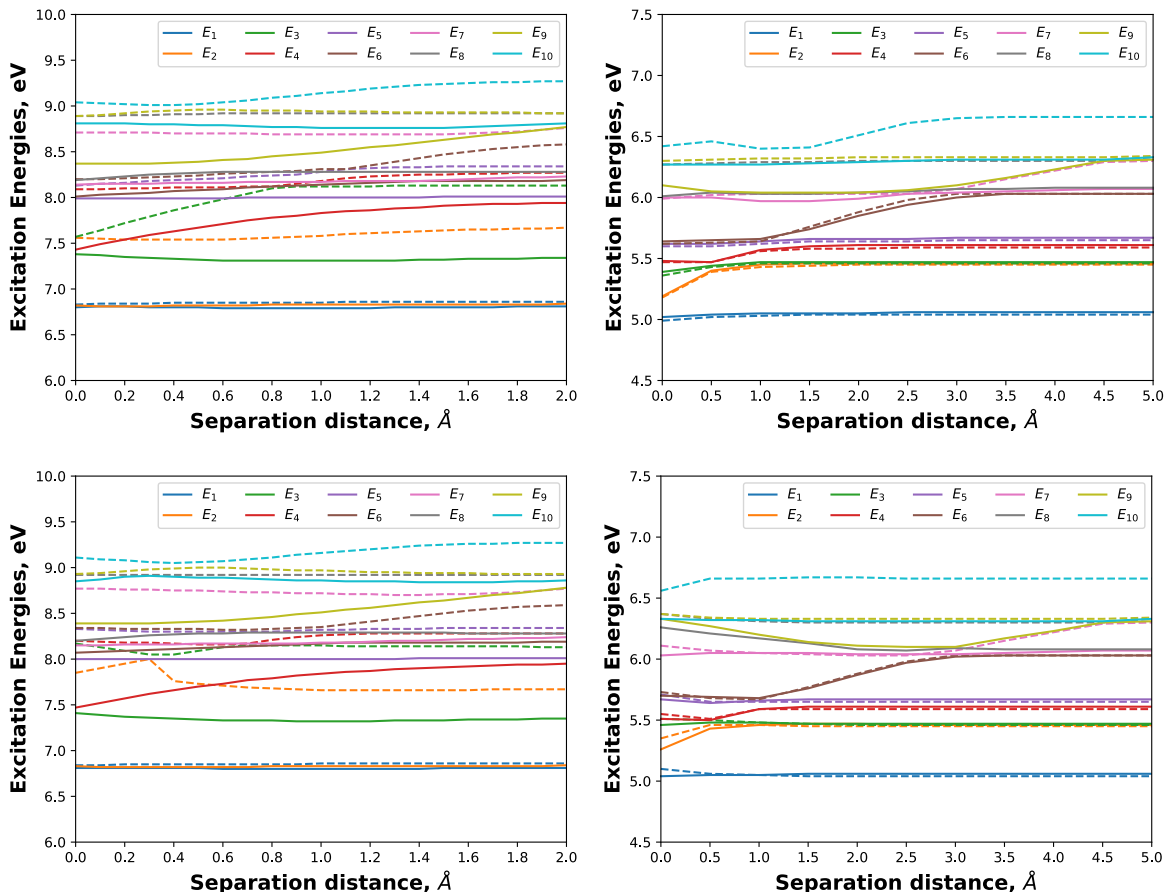


FIG. 10: Top panel: Excitation energies of the lowest 10 supermolecular states in the CMO basis from AMS (full lines) and SERENITY (dashed lines) using TDA with respect to the separation distance of the  $C_2H_4 - C_2F_4$  (left panel) and adenine-thymine (right panel) dimers. Bottom panel: Excitation energies of the lowest 10 adiabatic states obtained by RD pathway with  $M = 80$  diabatic states from RILMO-TDA (full lines) and PbE-sTDA (dashed lines) for both dimers.

pled via RD. This gives a similar picture as seen for the CMO calculations, with relatively small deviations for the adenine-thymine dimer and larger deviations for the  $C_2H_4 - C_2F_4$  dimer.

### C. Application to a *chlorophyll a* dimer in Light Harvesting Complex II

After this assessment of the RILMO-TDA approach, we now provide an application to molecules of biological importance. We choose a dimer consisting of chlorophyll molecules, that has been studied previously by some of us<sup>118</sup> using subsystem DFT. In this work, we used the traditional version with non-additive kinetic energy functionals as opposed to projection-based embedding. This particular dimer is known to play a crucial role in light-induced energy transfer processes in light-harvesting complexes in higher plants<sup>118,119</sup>. In this previous work, we observed an increase in the mixing of charge-transfer states with the local states upon a decrease in the distance between the two

chromophores. A direct manifestation of this mixing is the red-shifting of the lowest excited states and a decrease in the total oscillator strength. To study this mixing with the current method that offers an easy analysis of the effect of CT, we seek to calculate the uLE and uCT states along with their corresponding electronic couplings for two representative structures. In conformation 1 the distance between the two chlorophylls is relatively large, while in conformation 2 the two chlorophylls are stacked at relatively close distance (see Fig. 3c).

The CAM-B3LYP exchange-correlation functional along with the Slater-type basis set DZP was used for this system, while we performed Gaussian-type def2-SVP with SERENITY for comparison. Here again, the full virtual space was retained (no RILMO truncation) for comparison purposes.

The RILMOs and orbitals from PbE-sDFT corresponding to the HOMO ( $\pi$ ) and LUMO ( $\pi^*$ ) for the two chlorophyll molecules in conformation 2 are shown in Fig. 13. The supermolecular CMOs are also shown for reference. As can be seen, the canonical HOMOs are delocalized over both

TABLE I: uLE energies of the  $C_2H_4 - C_2F_4$  dimer obtained from RILMO-TDA and PbE-sTDA methods at varying distances  $d$  (Å). Also shown are the isolated fragment energies. All units are in eV.

		$d = 0$	$d = 0.5$	$d = 1.0$	$d = 1.5$	$d = 2.0$	isolated
<b>RILMO-TDA</b>	<b>uLE<sub>1</sub></b>	8.33	8.31	8.30	8.29	8.28	8.28
	<b>uLE<sub>2</sub></b>	9.03	9.02	9.00	9.00	8.99	8.99
<b>PbE-sTDA</b>	<b>uLE<sub>1</sub></b>	8.49	8.39	8.34	8.31	8.29	8.29
	<b>uLE<sub>2</sub></b>	9.03	8.97	8.94	8.92	8.91	8.91

TABLE II: uLE energies of the adenine-thymine dimer obtained from RILMO-TDA and PbE-sTDA methods at varying distances  $d$  (Å). Also shown are the isolated fragment energies. All units are in eV.

		$d = 0$	$d = 1.0$	$d = 2.0$	$d = 3.0$	$d = 4.0$	isolated
<b>RILMO-TDA</b>	<b>uLE<sub>1a</sub></b>	5.72	5.69	5.68	5.67	5.67	5.67
	<b>uLE<sub>1b</sub></b>	5.64	5.62	5.61	5.61	5.61	5.61
	<b>uLE<sub>2</sub></b>	5.51	5.48	5.47	5.47	5.47	5.48
<b>PbE-sTDA</b>	<b>uLE<sub>1a</sub></b>	5.75	5.67	5.65	5.65	5.65	5.65
	<b>uLE<sub>1b</sub></b>	5.69	5.60	5.59	5.59	5.59	5.59
	<b>uLE<sub>2</sub></b>	5.55	5.47	5.45	5.45	5.45	5.46

fragments, and localization (followed by re-canonicalization) helps to retain the delocalized nature of the  $\pi$  and  $\pi^*$  orbitals localized over each fragment.

Employing these localized orbitals, we carried out RILMO-TDA calculations for the uLE and uCT states. In order to demonstrate the flexibility of such an approach for this system, we also used Grimme’s simplified TDA<sup>106</sup> approach (RILMO-simTDA) to calculate the uncoupled excitation energies and the electronic couplings given by Eq. (27). The transitions considered in the uLE and uCT subspaces for the dimer consist of two lowest  $\pi \rightarrow \pi^*$  transitions of LE type for each of the chlorophyll, CLA1 and CLA2 (denoted as uLE<sub>1</sub> and uLE<sub>2</sub> respectively), and two lowest  $\pi \rightarrow \pi^*$  of CT type – CLA1  $\rightarrow$  CLA2 and CLA2  $\rightarrow$  CLA1 (denoted as uCT<sub>1</sub> and uCT<sub>2</sub> respectively). Table III lists these energies for two of the conformations shown in Fig. 3c, using both of these methods and PbE-sTDA. Although the full TDA and simplified TDA methods present some differences in the excitation energies, they both predict a distinct drop in the CT energies for conformation 2, although the latter yields a more drastic change probably owing to the approximations introduced in the calculation of the coupling elements of the  $\mathbf{A}$  matrix for simplified TDA.

The effect of the truncation of the size of the virtual space on the uLE and the uCT energies for both the conformations showed a similar trend as before, with the uLE energies displaying a gradual convergence behaviour with the increase in the number of virtual orbitals, and the uCT energies showing little to no change (see Fig. S7 in SI). Thus, overall, the RILMO-TDA excitation energies are in reasonable agreement with those of PbE-sTDA. Table IV also lists the corresponding couplings between the uLE and uCT states calculated from RILMO-TDA and RILMO-simTDA approaches. Although

there are minor differences between these two methods, the couplings of RILMO-TDA are in excellent agreement with that of PbE-sTDA. Furthermore, the truncation of the size of the virtual space shows no discernible changes in the couplings (see Fig. S8 in the SI).

## V. CONCLUSIONS

In this work, we presented a simple one-step embedding approach for generating a set of re-canonicalized intrinsic localized molecular orbitals (RILMOs) for each fragment starting from a set of canonical molecular orbitals (CMOs). As an extension to the valence ILMOs discussed in our previous work<sup>94</sup>, these orbital sets include also the so-called hard virtual orbitals that are needed for a quantitative description of electronically excited states. While fully localized on individual fragments, RILMOs are delocalized within a fragment and can thus retain the intrinsic  $\pi$  and  $\pi^*$  character encountered in isolated conjugated systems. Since the ILMOs are orthogonal by construction, our procedure eliminates the need for the construction of any projection operators. Nevertheless, the orbitals are comparable to a set of polarized orthonormal orbitals arising from a top-down projection-based embedding procedure. We furthermore outlined a TDDFT strategy for obtaining LE and CT states and investigated the effect of truncating the size of the virtual space in the localization procedure on the energies of these states. While the diabatic LE energies displayed a relatively slow convergence behaviour upon increasing the total number of virtual orbitals in the localization step, the diabatic CT energies were found to converge very quickly. The excitation energies and electronic couplings obtained in this approximate diabatic basis of the LE and CT states are in reasonable agreement with

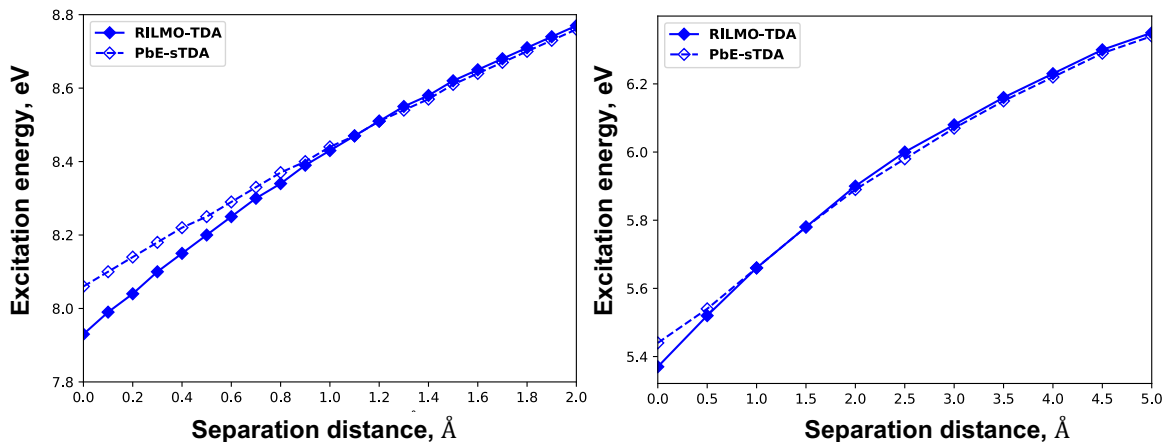


FIG. 11: uCT energies obtained from RILMO-TDA (full lines) and PbE-sTDA (dashed lines) as a function of the separation distance for the  $C_2H_4 - C_2F_4$  (left panel) and adenine-thymine (right panel) dimers.

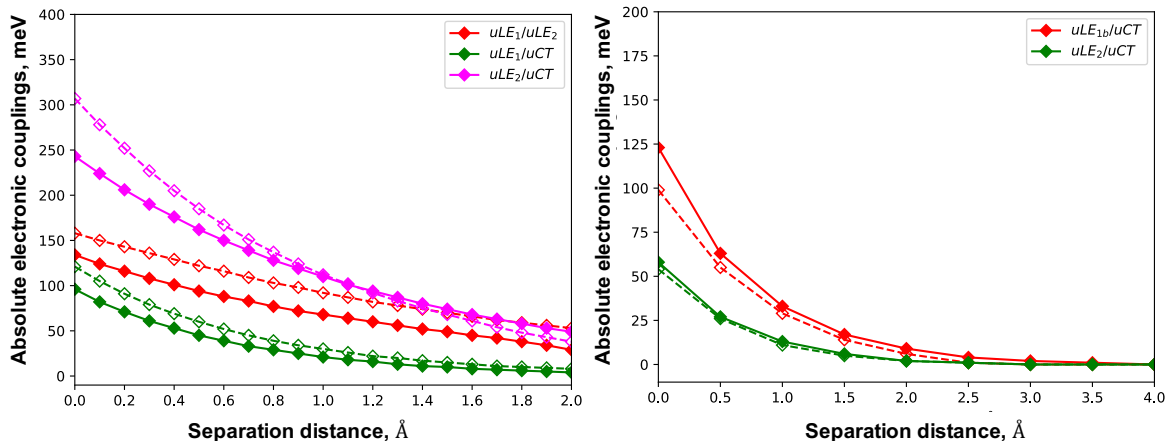


FIG. 12: Absolute electronic couplings between the uLE and uCT states from RILMO-TDA (full lines) and PbE-sTDA (dashed lines) as a function of the separation distance for the  $C_2H_4 - C_2F_4$  (left panel) and adenine-thymine (right panel) dimers.

those from subsystem DFT using projection-based embedding. Our observations are in accordance with previous studies that showed a similar dependence of the diabatic excitation energies and electronic couplings on the diabatization procedure employed.<sup>41,45</sup> Nonetheless, we believe that our procedure will be useful due to its simple implementation and possibilities for easy extension to other excited state methods (DFTB, BSE, equation-of-motion coupled cluster, etc). The current scheme can for instance be used as an analysis toolkit for studying ET and EET processes in photo-induced systems.

## SUPPLEMENTARY MATERIAL

See the supplementary material for 1) effect of truncation of virtual space on the uLE energies of isolated  $C_2H_4 - C_2F_4$  and adenine-thymine dimers, 2) effect of truncation of virtual

space on the electronic couplings of both of these dimers, 3) Convergence of the RILMO-TDA states in the CD and RD pathway for a water-ammonia dimer, 4) electronic couplings and orbital energies for both of these dimers with varying distances and 5) effect of truncation of virtual space on the uLE and uCT energies and electronic couplings of the chlorophyll dimer

## ACKNOWLEDGMENTS

The authors would like to thank Dr. Johannes Tölle for valuable discussions and Prof. Johannes Neugebauer for providing access to the ethylene-tetrafluoroethylene structure used in this work. S.S. and L.V. acknowledge support from NWO via the CSER program and for access to the National Computing Facilities.

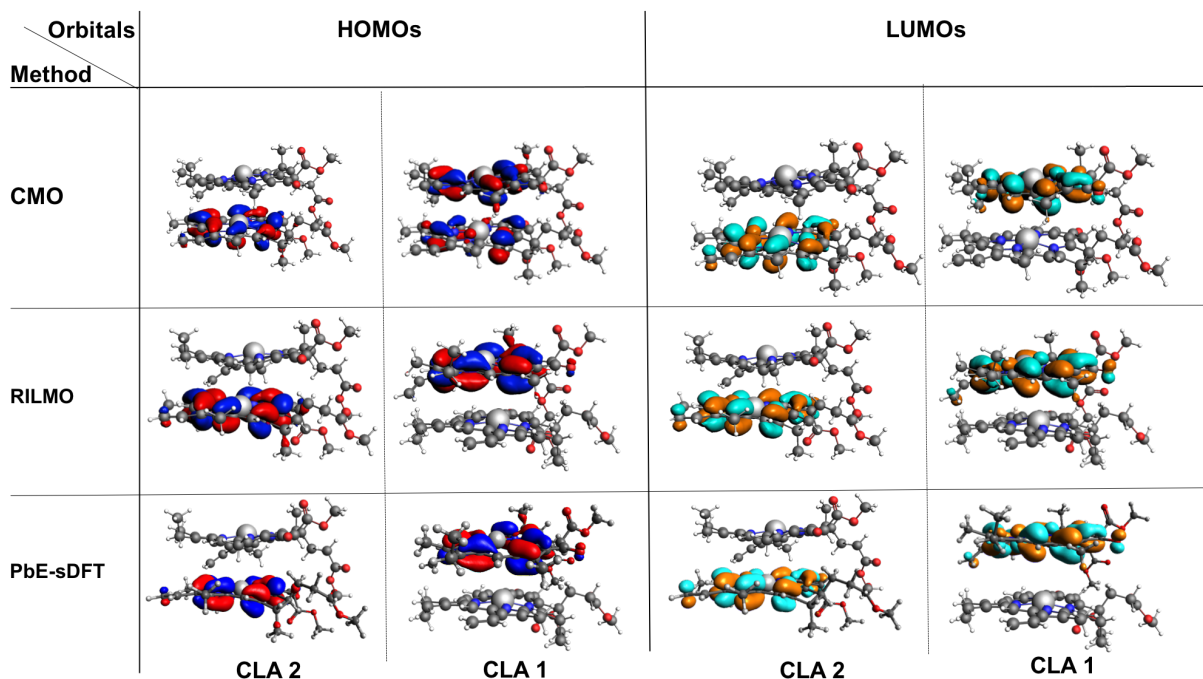


FIG. 13: HOMOs and LUMOs associated with the lowest  $\pi \rightarrow \pi^*$  transition for each of the chlorophyll molecules in conformation 2 (denoted as CLA1 and CLA2) from different set of orbitals: CMOs (top row), RILMOs (middle row) and orbitals from PbE-sDFT (bottom row).

## AUTHOR DECLARATIONS

### Conflict of Interest

The authors have no conflicts to disclose.

### Author Contributions

**Souloke Sen:** Data curation (lead); Investigation (equal); Methodology (equal); Validation (equal); Writing - original draft (lead). **Bruno Senjean:** Methodology (equal); Validation (equal); Writing - review & editing (equal). **Lucas Visscher:** Conceptualization (lead); Methodology (equal); Supervision (lead); Investigation (equal); Validation (equal); Writing - review & editing (equal).

### DATA AVAILABILITY

The data used in this work are available upon reasonable request.

## REFERENCES

- <sup>1</sup>M. E. Casida, "Time-dependent density functional response theory for molecules," in *Recent Advances In Density Functional Methods: (Part I)* (World Scientific, 1995) pp. 155–192.
- <sup>2</sup>M. Petersilka, U. Gossmann, and E. Gross, "Excitation energies from time-dependent density-functional theory," *Physical review letters* **76**, 1212 (1996).
- <sup>3</sup>N. T. Maitra, A. Wasserman, and K. Burke, "Successes and challenges," *Electron Correlations and Materials Properties 2*, 285 (2013).
- <sup>4</sup>M. A. Marques and E. K. Gross, "Time-dependent density functional theory," *Annu. Rev. Phys. Chem.* **55**, 427–455 (2004).
- <sup>5</sup>S. Van Gisbergen, J. Snijders, and E. Baerends, "Implementation of time-dependent density functional response equations," *Computer Physics Communications* **118**, 119–138 (1999).
- <sup>6</sup>W. Kohn and L. J. Sham, "Self-consistent equations including exchange and correlation effects," *Physical review* **140**, A1133 (1965).
- <sup>7</sup>A. Dreuw and M. Head-Gordon, "Single-reference ab initio methods for the calculation of excited states of large molecules," *Chemical reviews* **105**, 4009–4037 (2005).
- <sup>8</sup>M. E. Casida, "Time-dependent density-functional theory for molecules and molecular solids," *Journal of Molecular Structure: THEOCHEM* **914**, 3–18 (2009).
- <sup>9</sup>J. Liu and W. Liang, "Analytical approach for the excited-state hessian in time-dependent density functional theory: Formalism, implementation, and performance," *The Journal of chemical physics* **135**, 184111 (2011).
- <sup>10</sup>R. Sarkar, M. Boggio-Pasqua, P.-F. Loos, and D. Jacquemin, "Benchmarking td-dft and wave function methods for oscillator strengths and excited-

TABLE III: uLE and uCT energies of the chlorophyll dimer obtained from PbE-sTDA, RILMO-TDA and RILMO-simTDA methods for both conformations. All units are in eV.

	States	PbE-sTDA	RILMO-TDA	RILMO-simTDA
<b>Conformation 1</b>	uLE <sub>1</sub>	2.21	2.22	1.93
	uLE <sub>2</sub>	2.25	2.26	1.96
	uCT <sub>1</sub>	2.82	2.80	2.36
	uCT <sub>2</sub>	2.97	2.97	2.54
<b>Conformation 2</b>	uLE <sub>1</sub>	2.31	2.27	1.98
	uLE <sub>2</sub>	2.25	2.25	1.96
	uCT <sub>1</sub>	2.70	2.67	2.22
	uCT <sub>2</sub>	2.30	2.24	1.79

TABLE IV: Absolute electronic couplings between the uLE/uCT states of the chlorophyll dimer obtained from PbE-sTDA, RILMO-TDA and RILMO-simTDA methods for both conformations. All units are in meV.

	States	PbE-sTDA	RILMO-TDA	RILMO-simTDA
<b>Conformation 1</b>	uLE <sub>1</sub> /uLE <sub>2</sub>	27	26	35
	uLE <sub>1</sub> /uCT <sub>1</sub>	7	8	9
	uLE <sub>1</sub> /uCT <sub>2</sub>	20	20	20
	uLE <sub>2</sub> /uCT <sub>1</sub>	19	17	17
	uLE <sub>2</sub> /uCT <sub>2</sub>	7	8	9
<b>Conformation 2</b>	uLE <sub>1</sub> /uLE <sub>2</sub>	36	36	44
	uLE <sub>1</sub> /uCT <sub>1</sub>	27	29	28
	uLE <sub>1</sub> /uCT <sub>2</sub>	44	44	45
	uLE <sub>2</sub> /uCT <sub>1</sub>	31	29	37
	uLE <sub>2</sub> /uCT <sub>2</sub>	23	21	19

state dipole moments,” *Journal of Chemical Theory and Computation* **17**, 1117–1132 (2021).

- <sup>11</sup>Y. Tawada, T. Tsuneda, S. Yanagisawa, T. Yanai, and K. Hirao, “A long-range-corrected time-dependent density functional theory,” *The Journal of chemical physics* **120**, 8425–8433 (2004).
- <sup>12</sup>H. Iikura, T. Tsuneda, T. Yanai, and K. Hirao, “A long-range correction scheme for generalized-gradient-approximation exchange functionals,” *The Journal of Chemical Physics* **115**, 3540–3544 (2001).
- <sup>13</sup>T. Yanai, D. P. Tew, and N. C. Handy, “A new hybrid exchange–correlation functional using the coulomb-attenuating method (cam-b3lyp),” *Chemical physics letters* **393**, 51–57 (2004).
- <sup>14</sup>T. Stein, L. Kronik, and R. Baer, “Reliable prediction of charge transfer excitations in molecular complexes using time-dependent density functional theory,” *Journal of the American Chemical Society* **131**, 2818–2820 (2009).
- <sup>15</sup>A. D. Laurent and D. Jacquemin, “Td-dft benchmarks: a review,” *International Journal of Quantum Chemistry* **113**, 2019–2039 (2013).
- <sup>16</sup>H. Li, R. Nieman, A. J. Aquino, H. Lischka, and S. Tretiak, “Comparison of lc-tddft and adc (2) methods in computations of bright and charge transfer states in stacked oligothiophenes,” *Journal of chemical theory and computation* **10**, 3280–3289 (2014).
- <sup>17</sup>B. Moore, H. Sun, N. Govind, K. Kowalski, and J. Autschbach, “Charge-transfer versus charge-transfer-like excitations revisited,” *Journal of chemical theory and computation* **11**, 3305–3320 (2015).
- <sup>18</sup>M. Wormit, *Development and application of reliable methods for the calculation of excited states: From light-harvesting complexes to medium-sized molecules*, Ph.D. thesis, Citeseer (2009).
- <sup>19</sup>M. Wanko, M. Hoffmann, P. Strodel, A. Koslowski, W. Thiel, F. Neese, T. Frauenheim, and M. Elstner, “Calculating absorption shifts for retinal proteins: computational challenges,” *The Journal of Physical Chemistry B* **109**, 3606–3615 (2005).
- <sup>20</sup>D. Jacquemin, E. A. Perpète, G. Scalmani, M. J. Frisch, R. Kobayashi, and C. Adamo, “Assessment of the efficiency of long-range corrected functionals for some properties of large compounds,” *The Journal of chemical physics* **126**, 144105 (2007).
- <sup>21</sup>D. Jacquemin, E. A. Perpète, G. E. Scuseria, I. Ciofini, and C. Adamo, “Td-dft performance for the visible absorption spectra of organic dyes: conventional versus long-range hybrids,” *Journal of chemical theory and computation* **4**, 123–135 (2008).
- <sup>22</sup>C. Curutchet and B. Mennucci, “Quantum chemical studies of light harvesting,” *Chemical reviews* **117**, 294–343 (2017).
- <sup>23</sup>C. König and J. Neugebauer, “Quantum chemical description of absorption properties and excited-state processes in photosynthetic systems,” *ChemPhysChem* **13**, 386–425 (2012).
- <sup>24</sup>N. S. Sariciftci, L. Smilowitz, A. J. Heeger, and F. Wudl, “Photoinduced electron transfer from a conducting polymer to buckminsterfullerene,” *Science* **258**, 1474–1476 (1992).
- <sup>25</sup>R. Blankenship, “Molecular mechanisms of photosynthesis blackwell science,” Maiden, MA (2002).
- <sup>26</sup>F. Segatta, L. Cupellini, M. Garavelli, and B. Mennucci, “Quantum chemical modeling of the photoinduced activity of multichromophoric biosystems: Focus review,” *Chemical reviews* **119**, 9361–9380 (2019).
- <sup>27</sup>V. I. Novoderezhkin and R. van Grondelle, “Physical origins and models of energy transfer in photosynthetic light-harvesting,” *Physical Chemistry Chemical Physics* **12**, 7352–7365 (2010).
- <sup>28</sup>H. van Amerongen and R. van Grondelle, “Understanding the energy transfer function of lhci<sub>ii</sub>, the major light-harvesting complex of green plants,” (2001).
- <sup>29</sup>V. I. Novoderezhkin, J. P. Dekker, and R. Van Grondelle, “Mixing of exciton and charge-transfer states in photosystem ii reaction centers: modeling of stark spectra with modified redfield theory,” *Biophysical journal* **93**, 1293–1311 (2007).
- <sup>30</sup>V. I. Novoderezhkin, E. G. Andrizhievskaya, J. P. Dekker, and R. van Grondelle, “Pathways and timescales of primary charge separation in the photosystem ii reaction center as revealed by a simultaneous fit of time-resolved fluorescence and transient absorption,” *Biophysical journal* **89**,

- 1464–1481 (2005).
- <sup>31</sup>J. Frenkel, “On the transformation of light into heat in solids. i,” *Physical Review* **37**, 17 (1931).
- <sup>32</sup>A. S. Davydov, “The theory of molecular excitons,” *Soviet Physics Uspekhi* **7**, 145 (1964).
- <sup>33</sup>D. Abramavicius, B. Palmieri, D. V. Voronine, F. Sanda, and S. Mukamel, “Coherent multidimensional optical spectroscopy of excitons in molecular aggregates; quasiparticle versus supermolecule perspectives,” *Chemical reviews* **109**, 2350–2408 (2009).
- <sup>34</sup>A. F. Morrison, Z.-Q. You, and J. M. Herbert, “Ab initio implementation of the frenkel–davydov exciton model: a naturally parallelizable approach to computing collective excitations in crystals and aggregates,” *Journal of Chemical Theory and Computation* **10**, 5366–5376 (2014).
- <sup>35</sup>Y. Ma and H. Ma, “Calculating excited states of molecular aggregates by the renormalized excitonic method,” *The Journal of Physical Chemistry A* **117**, 3655–3665 (2013).
- <sup>36</sup>Y. Ma, Y. Liu, and H. Ma, “A new fragment-based approach for calculating electronic excitation energies of large systems,” *The Journal of Chemical Physics* **136**, 024113 (2012).
- <sup>37</sup>S. Tretiak, W. M. Zhang, V. Chernyak, and S. Mukamel, “Excitonic couplings and electronic coherence in bridged naphthalene dimers,” *Proceedings of the National Academy of Sciences* **96**, 13003–13008 (1999).
- <sup>38</sup>X. Li, R. M. Parrish, F. Liu, S. I. Kokkila Schumacher, and T. J. Martínez, “An ab initio exciton model including charge-transfer excited states,” *Journal of chemical theory and computation* **13**, 3493–3504 (2017).
- <sup>39</sup>Y. Kurihara, Y. Aoki, and A. Imamura, “Calculations of the excitation energies of all-trans and 11, 12s-dicis retinals using localized molecular orbitals obtained by the elongation method,” *The Journal of chemical physics* **107**, 3569–3575 (1997).
- <sup>40</sup>T. D. Bouman, B. Voigt, and A. E. Hansen, “Optical activity of saturated ketones. ab initio localized orbital analysis of a model ketone in the random-phase approximation,” *Journal of the American Chemical Society* **101**, 550–558 (1979).
- <sup>41</sup>W. Liu, B. Lunkenheimer, V. Settels, B. Engels, R. F. Fink, and A. Köhn, “A general ansatz for constructing quasi-diabatic states in electronically excited aggregated systems,” *The Journal of chemical physics* **143**, 084106 (2015).
- <sup>42</sup>D. Accomasso, M. Persico, and G. Granucci, “Diabatization by localization in the framework of configuration interaction based on floating occupation molecular orbitals (fomo-ci),” *ChemPhotoChem* **3**, 933–944 (2019).
- <sup>43</sup>R. Cimraglia, J.-P. Malrieu, M. Persico, and F. Spiegelmann, “Quasi-diabatic states and dynamical couplings from ab initio ci calculations: a new proposal,” *Journal of Physics B: Atomic and Molecular Physics* (1968-1987) **18**, 3073 (1985).
- <sup>44</sup>M. Nottoli, S. Jurinovich, L. Cupellini, A. T. Gardiner, R. Cogdell, and B. Mennucci, “The role of charge-transfer states in the spectral tuning of antenna complexes of purple bacteria,” *Photosynthesis research* **137**, 215–226 (2018).
- <sup>45</sup>J. Tölle, L. Cupellini, B. Mennucci, and J. Neugebauer, “Electronic couplings for photo-induced processes from subsystem time-dependent density-functional theory: The role of the diabatization,” *The Journal of Chemical Physics* **153**, 184113 (2020).
- <sup>46</sup>Y. G. Khait and M. R. Hoffmann, “Embedding theory for excited states,” *The Journal of chemical physics* **133**, 044107 (2010).
- <sup>47</sup>Q. Sun and G. K.-L. Chan, “Quantum embedding theories,” *Accounts of chemical research* **49**, 2705–2712 (2016).
- <sup>48</sup>T. A. Wesolowski, “Embedding a multideterminantal wave function in an orbital-free environment,” *Physical Review A* **77**, 012504 (2008).
- <sup>49</sup>T. A. Wesolowski, “Embedding potentials for excited states of embedded species,” *The Journal of Chemical Physics* **140**, 18A530 (2014).
- <sup>50</sup>T. A. Wesolowski, S. Shedge, and X. Zhou, “Frozen-density embedding strategy for multilevel simulations of electronic structure,” *Chemical reviews* **115**, 5891–5928 (2015).
- <sup>51</sup>C. Daday, C. Kofiig, O. Vålsson, J. Neugebauer, and C. Filippi, “State-specific embedding potentials for excitation-energy calculations,” *Journal of chemical theory and computation* **9**, 2355–2367 (2013).
- <sup>52</sup>S. Höfener, A. Severo Pereira Gomes, and L. Visscher, “Molecular properties via a subsystem density functional theory formulation: A common framework for electronic embedding,” *The Journal of chemical physics* **136**, 044104 (2012).
- <sup>53</sup>X. Wen, D. S. Graham, D. V. Chulhai, and J. D. Goodpaster, “Absolutely localized projection-based embedding for excited states,” *Journal of Chemical Theory and Computation* **16**, 385–398 (2019).
- <sup>54</sup>D. V. Chulhai and L. Jensen, “External orthogonality in subsystem time-dependent density functional theory,” *Physical Chemistry Chemical Physics* **18**, 21032–21039 (2016).
- <sup>55</sup>J. D. Goodpaster, T. A. Barnes, and T. F. Miller III, “Embedded density functional theory for covalently bonded and strongly interacting subsystems,” *The Journal of chemical physics* **134**, 164108 (2011).
- <sup>56</sup>F. Libisch, C. Huang, and E. A. Carter, “Embedded correlated wavefunction schemes: Theory and applications,” *Accounts of chemical research* **47**, 2768–2775 (2014).
- <sup>57</sup>G. Senatore and K. Subbaswamy, “DENSITY DEPENDENCE OF THE DIELECTRIC-CONSTANT OF RARE-GAS CRYSTALS,” *Physical Review B* **34**, 5754 – 5757 (1986).
- <sup>58</sup>P. Cortona, “Self-consistently determined properties of solids without band-structure calculations,” *Physical Review B* **44**, 8454 (1991).
- <sup>59</sup>T. A. Wesolowski and A. Warshel, “Frozen density functional approach for ab initio calculations of solvated molecules,” *The Journal of Physical Chemistry* **97**, 8050–8053 (1993).
- <sup>60</sup>C. R. Jacob and J. Neugebauer, “Subsystem density-functional theory,” *Wiley Interdisciplinary Reviews: Computational Molecular Science* **4**, 325–362 (2014).
- <sup>61</sup>P. K. Tamukong, Y. G. Khait, and M. R. Hoffmann, “Density differences in embedding theory with external orbital orthogonality,” *The Journal of Physical Chemistry A* **118**, 9182–9200 (2014).
- <sup>62</sup>D. V. Chulhai and L. Jensen, “Frozen density embedding with external orthogonality in delocalized covalent systems,” *Journal of chemical theory and computation* **11**, 3080–3088 (2015).
- <sup>63</sup>P. K. Tamukong, Y. G. Khait, and M. R. Hoffmann, “Accurate dissociation of chemical bonds using dft-in-dft embedding theory with external orbital orthogonality,” *The Journal of Physical Chemistry A* **121**, 256–264 (2017).
- <sup>64</sup>K. Kiewisch, G. Eickerling, M. Reiher, and J. Neugebauer, “Topological analysis of electron densities from kohn-sham and subsystem density functional theory,” *The Journal of chemical physics* **128**, 044114 (2008).
- <sup>65</sup>M. E. Casida and T. A. Wesolowski, “Generalization of the kohn-sham equations with constrained electron density formalism and its time-dependent response theory formulation,” *International journal of quantum chemistry* **96**, 577–588 (2004).
- <sup>66</sup>J. Neugebauer, “Couplings between electronic transitions in a subsystem formulation of time-dependent density functional theory,” *The Journal of chemical physics* **126**, 134116 (2007).
- <sup>67</sup>C. König, N. Schlüter, and J. Neugebauer, “Direct determination of exciton couplings from subsystem time-dependent density-functional theory within the tamm–dancoff approximation,” *The Journal of chemical physics* **138**, 034104 (2013).
- <sup>68</sup>J. Neugebauer, “Subsystem-based theoretical spectroscopy of biomolecules and biomolecular assemblies,” *ChemPhysChem* **10**, 3148–3173 (2009).
- <sup>69</sup>J. Neugebauer, “Photophysical properties of natural light-harvesting complexes studied by subsystem density functional theory,” *The Journal of Physical Chemistry B* **112**, 2207–2217 (2008).
- <sup>70</sup>J. Tölle and J. Neugebauer, “The seamless connection of local and collective excited states in subsystem time-dependent density functional theory,” *The Journal of Physical Chemistry Letters* **13**, 1003–1018 (2022).
- <sup>71</sup>T. Dresselhaus and J. Neugebauer, “Part and whole in wavefunction/dft embedding,” *Theoretical Chemistry Accounts* **134**, 1–15 (2015).
- <sup>72</sup>J. Foster and S. Boys, “Canonical configurational interaction procedure,” *Rev. Mod. Phys.* **32**, 300 (1960).
- <sup>73</sup>C. Edmiston and K. Ruedenberg, “Localized atomic and molecular orbitals,” *Rev. Mod. Phys.* **35**, 457 (1963).
- <sup>74</sup>J. Pipek and P. G. Mezey, “A fast intrinsic localization procedure applicable for abinitio and semiempirical linear combination of atomic orbital wave functions,” *The Journal of Chemical Physics* **90**, 4916–4926 (1989).
- <sup>75</sup>G. Knizia, “Intrinsic atomic orbitals: An unbiased bridge between quantum theory and chemical concepts,” *Journal of chemical theory and computation* **9**, 4834–4843 (2013).
- <sup>76</sup>S. J. Lee, M. Welborn, F. R. Manby, and T. F. Miller III, “Projection-based wavefunction-in-dft embedding,” *Accounts of chemical research* **52**,

- 1359–1368 (2019).
- <sup>77</sup>S. J. Bennie, B. F. Curchod, F. R. Manby, and D. R. Glowacki, “Pushing the limits of eom-ccsd with projector-based embedding for excitation energies,” *The Journal of Physical Chemistry Letters* **8**, 5559–5565 (2017).
- <sup>78</sup>B. Hégyely, P. R. Nagy, G. G. Ferenczy, and M. Kállay, “Exact density functional and wave function embedding schemes based on orbital localization,” *The Journal of Chemical Physics* **145**, 064107 (2016).
- <sup>79</sup>J. Tölle, M. Böckers, N. Niemeier, and J. Neugebauer, “Inter-subsystem charge-transfer excitations in exact subsystem time-dependent density-functional theory,” *The Journal of chemical physics* **151**, 174109 (2019).
- <sup>80</sup>T. M. Henderson, “Embedding wave function theory in density functional theory,” *The Journal of chemical physics* **125**, 014105 (2006).
- <sup>81</sup>J. E. Subotnik, S. Yeganeh, R. J. Cave, and M. A. Ratner, “Constructing diabatic states from adiabatic states: Extending generalized mulliken–hush to multiple charge centers with boys localization,” *The Journal of chemical physics* **129**, 244101 (2008).
- <sup>82</sup>J. E. Subotnik, R. J. Cave, R. P. Steele, and N. Shenoi, “The initial and final states of electron and energy transfer processes: Diabatization as motivated by system-solvent interactions,” *The Journal of chemical physics* **130**, 234102 (2009).
- <sup>83</sup>M. Pavanello and J. Neugebauer, “Linking the historical and chemical definitions of diabatic states for charge and excitation energy transfer reactions in condensed phase,” *The Journal of chemical physics* **135**, 134113 (2011).
- <sup>84</sup>J. Tölle, M. Böckers, and J. Neugebauer, “Exact subsystem time-dependent density-functional theory,” *The Journal of chemical physics* **150**, 181101 (2019).
- <sup>85</sup>L. Scholz, J. Tölle, and J. Neugebauer, “Analysis of environment response effects on excitation energies within subsystem-based time-dependent density-functional theory,” *International Journal of Quantum Chemistry*, e26213 (2020).
- <sup>86</sup>M. Bensberg and J. Neugebauer, “Automatic basis-set adaptation in projection-based embedding,” *The Journal of chemical physics* **150**, 184104 (2019).
- <sup>87</sup>A. A. Voityuk and N. Rösch, “Fragment charge difference method for estimating donor–acceptor electronic coupling: Application to dna  $\pi$ -stacks,” *The Journal of chemical physics* **117**, 5607–5616 (2002).
- <sup>88</sup>C.-P. Hsu, Z.-Q. You, and H.-C. Chen, “Characterization of the short-range couplings in excitation energy transfer,” *The Journal of Physical Chemistry C* **112**, 1204–1212 (2008).
- <sup>89</sup>C.-H. Yang and C.-P. Hsu, “A multi-state fragment charge difference approach for diabatic states in electron transfer: Extension and automation,” *The Journal of Chemical Physics* **139**, 154104 (2013).
- <sup>90</sup>L. Cupellini, D. Calvani, D. Jacquemin, and B. Mennucci, “Charge transfer from the carotenoid can quench chlorophyll excitation in antenna complexes of plants,” *Nature communications* **11**, 1–8 (2020).
- <sup>91</sup>L. Cupellini, S. Caprasecca, C. A. Guido, F. Muñ, T. Renger, and B. Mennucci, “Coupling to charge transfer states is the key to modulate the optical bands for efficient light harvesting in purple bacteria,” *The Journal of Physical Chemistry Letters* **9**, 6892–6899 (2018).
- <sup>92</sup>F. Wu, W. Liu, Y. Zhang, and Z. Li, “Linear-scaling time-dependent density functional theory based on the idea of “from fragments to molecule,”” *Journal of Chemical Theory and Computation* **7**, 3643–3660 (2011).
- <sup>93</sup>M. Miura and Y. Aoki, “Ab initio theory for treating local electron excitations in molecules and its performance for computing optical properties,” *Journal of computational chemistry* **30**, 2213–2230 (2009).
- <sup>94</sup>B. Senjean, S. Sen, M. Repisky, G. Knizia, and L. Visscher, “Generalization of intrinsic orbitals to kramers-paired quaternion spinors, molecular fragments, and valence virtual spinors,” *Journal of chemical theory and computation* **17**, 1337–1354 (2021).
- <sup>95</sup>Y. G. Khait and M. R. Hoffmann, “On the orthogonality of orbitals in subsystem kohn–sham density functional theory,” in *Annual Reports in Computational Chemistry*, Vol. 8 (Elsevier, 2012) pp. 53–70.
- <sup>96</sup>I. Tamm, “Relativistic interaction of elementary particles,” *J.Phys.(USSR)* **9**, 449 (1945); S. Dancoff, “Non-adiabatic meson theory of nuclear forces,” *Physical Review* **78**, 382 (1950).
- <sup>97</sup>A. Zangwill and P. Soven, “Resonant photoemission in barium and cerium,” *Physical Review Letters* **45**, 204 (1980).
- <sup>98</sup>E. Gross and W. Kohn, “Local density-functional theory of frequency-dependent linear response,” *Physical review letters* **55**, 2850 (1985).
- <sup>99</sup>R. Bauernschmitt and R. Ahlrichs, “Treatment of electronic excitations within the adiabatic approximation of time dependent density functional theory,” *Chemical Physics Letters* **256**, 454–464 (1996).
- <sup>100</sup>Z. Li, H. Li, B. Suo, and W. Liu, “Localization of Molecular Orbitals: From Fragments to Molecule,” *Accounts of Chemical Research* **47**, 2758–2767 (2014).
- <sup>101</sup>J. E. Subotnik, A. D. Dutoi, and M. Head-Gordon, “Fast localized orthonormal virtual orbitals which depend smoothly on nuclear coordinates,” *The Journal of Chemical Physics* **123**, 114108 (2005).
- <sup>102</sup>R. S. Mulliken, “Electronic population analysis on lcao–mo molecular wave functions. i,” *The Journal of Chemical Physics* **23**, 1833–1840 (1955).
- <sup>103</sup>E. Davidson, “The iterative calculation of a few of the lowest eigenvalues and corresponding eigenvectors of large real-symmetric matrices,” *Journal of Computational Physics* **17**, 87–94 (1975).
- <sup>104</sup>M. Franchini, P. H. T. Philipsen, E. van Lenthe, and L. Visscher, “Accurate coulomb potentials for periodic and molecular systems through density fitting,” *Journal of chemical theory and computation* **10**, 1994–2004 (2014).
- <sup>105</sup>A. Förster, M. Franchini, E. van Lenthe, and L. Visscher, “A quadratic pair atomic resolution of the identity based sos-ao-mp2 algorithm using slater type orbitals,” *Journal of chemical theory and computation* **16**, 875–891 (2020).
- <sup>106</sup>S. Grimme, “A simplified tamm-dancoff density functional approach for the electronic excitation spectra of very large molecules,” *The Journal of chemical physics* **138**, 244104 (2013).
- <sup>107</sup>G. t. Te Velde, F. M. Bickelhaupt, E. J. Baerends, C. Fonseca Guerra, S. J. van Gisbergen, J. G. Snijders, and T. Ziegler, “Chemistry with adf,” *Journal of Computational Chemistry* **22**, 931–967 (2001).
- <sup>108</sup>E. Baerends, T. Ziegler, A. Atkins, J. Autschbach, O. Baseggio, D. Bashford, A. Bérces, F. Bickelhaupt, C. Bo, P. Boerrigter, L. Cavallo, C. Daul, D. Chong, D. Chulhai, L. Deng, R. Dickson, J. Dieterich, D. Ellis, M. van Faassen, L. Fan, T. Fischer, A. Förster, C. F. Guerra, M. Franchini, A. Ghysels, A. Giammona, S. van Gisbergen, A. Goetz, A. Götz, J. Groeneveld, O. Gritsenko, M. Grüning, S. Gusarov, F. Harris, P. van den Hoek, Z. Hu, C. Jacob, H. Jacobsen, L. Jensen, L. Joubert, J. Kaminski, G. van Kessel, C. König, F. Kootstra, A. Kovalenko, M. Krykunov, E. van Lenthe, D. McCormack, A. Michalak, M. Mitoraj, S. Morton, J. Neugebauer, V. Nicu, L. Noodleman, V. Osinga, S. Patchkovskii, M. Pavanello, C. Peeples, P. Philipsen, D. Post, C. Pye, H. Ramanantoanina, P. Ramos, W. Ravenek, M. Reimann, J. Rodríguez, P. Ros, R. Rüger, P. Schipper, D. Schlüns, H. van Schoot, G. Schreckenbach, J. Seldenthuis, M. Seth, J. Snijders, M. Solà, M. Stener, M. Swart, D. Swerhone, V. Tognetti, G. te Velde, P. Vernooijs, L. Versluis, L. Visscher, O. Visser, F. Wang, T. Wesolowski, E. van Wezenbeek, G. Wiesenecker, S. Wolff, T. Woo, and A. Yakovlev, “AMS2021, SCM, Theoretical Chemistry, Vrije Universiteit, Amsterdam, The Netherlands, <https://www.scm.com>,”.
- <sup>109</sup>B. Senjean, S. Sen, M. Repisky, G. Knizia, and L. Visscher, [Online]. [https://gitlab.com/quantum\\_rose](https://gitlab.com/quantum_rose) (2020).
- <sup>110</sup>M. Handzlik, B. van Beek, P. Melix, R. Rüger, P. Schipper, D. Schlüns, and F. Zapata, “PLAMS2021, SCM, Theoretical Chemistry, Vrije Universiteit, Amsterdam, The Netherlands, <https://www.scm.com>, <https://github.com/SCM-NV/PLAMS>,”.
- <sup>111</sup>J. P. Unsleber, T. Dresselhaus, K. Klahr, D. Schnieders, M. B'ockers, D. Barton, and J. Neugebauer, “Serenity: A subsystem quantum chemistry program,” *J. Comput. Chem.* **39**, 788–798 (2018).
- <sup>112</sup>F. R. Manby, M. Stella, J. D. Goodpaster, and T. F. Miller III, “A simple, exact density-functional-theory embedding scheme,” *Journal of chemical theory and computation* **8**, 2564–2568 (2012).
- <sup>113</sup>K. Eichkorn, O. Treutler, H. Öhm, M. Häser, and R. Ahlrichs, “Auxiliary basis sets to approximate coulomb potentials,” *Chemical physics letters* **240**, 283–290 (1995).
- <sup>114</sup>F. Weigend, A. Köhn, and C. Hättig, “Efficient use of the correlation consistent basis sets in resolution of the identity mp2 calculations,” *The Journal of chemical physics* **116**, 3175–3183 (2002).
- <sup>115</sup>L. Blancafort and A. A. Voityuk, “Exciton delocalization, charge transfer, and electronic coupling for singlet excitation energy transfer between stacked nucleobases in dna: An ms-caspt2 study,” *The Journal of Chemical Physics* **140**, 03B602\_1 (2014).
- <sup>116</sup>R. Improta, F. Santoro, and L. Blancafort, “Quantum mechanical studies on the photophysics and the photochemistry of nucleic acids and nucle-

- obases,” *Chemical reviews* **116**, 3540–3593 (2016).
- <sup>117</sup>S. Sen and L. Visscher, “Towards the description of charge transfer states in solubilised lhci using subsystem dft,” *Photosynth. Res.* (2022).
- <sup>118</sup>S. Sen, V. Mascoli, N. Liguori, R. Croce, and L. Visscher, “Understanding the relation between structural and spectral properties of light-harvesting complex ii,” *The Journal of Physical Chemistry A* **125**, 4313–4322 (2021).
- <sup>119</sup>N. Liguori, X. Periole, S. J. Marrink, and R. Croce, “From light-harvesting to photoprotection: structural basis of the dynamic switch of the major antenna complex of plants (lhci),” *Scientific reports* **5**, 1–10 (2015).
- <sup>120</sup>M. Bockers and J. Neugebauer, “Excitation energies of embedded open-shell systems: Unrestricted frozen-density-embedding time-dependent density-functional theory,” *The Journal of chemical physics* **149**, 074102 (2018).
- <sup>121</sup>S. Hirata, M. Head-Gordon, and R. J. Bartlett, “Configuration interaction singles, time-dependent hartree–fock, and time-dependent density functional theory for the electronic excited states of extended systems,” *The Journal of Chemical Physics* **111**, 10774–10786 (1999).
- <sup>122</sup>R. E. Stratmann, G. E. Scuseria, and M. J. Frisch, “An efficient implementation of time-dependent density-functional theory for the calculation of excitation energies of large molecules,” *The Journal of chemical physics* **109**, 8218–8224 (1998).

# Supplementary Material

## Characterization of Excited States in Time-Dependent Density Functional Theory Using Localized Molecular Orbitals

Souloke Sen,<sup>†</sup> Bruno Senjean,<sup>‡</sup> and Lucas Visscher\*,<sup>¶</sup>

<sup>†</sup>*Division of Theoretical Chemistry, Faculty of Sciences, Vrije Universiteit Amsterdam, De  
Boelelaan 1083, 1081 HV Amsterdam, The Netherlands*

<sup>‡</sup>*ICGM, Université de Montpellier, CNRS, ENSCM, Montpellier, France*

<sup>¶</sup>*Amsterdam Center for Multiscale Modeling, Division of Theoretical Chemistry, Faculty  
of Sciences, Vrije Universiteit Amsterdam, De Boelelaan 1083, 1081 HV Amsterdam, The  
Netherlands*

E-mail: l.visscher@vu.nl

## Table of Contents:

1. Effect of truncating the virtual space on the uLE energies of the isolated $C_2H_4 - C_2F_4$ and adenine-thymine dimers	Pg. S3
2. Effect of truncating the virtual space on electronic couplings of the $C_2H_4 - C_2F_4$ and adenine-thymine dimers	Pg. S4
3. Convergence of the RILMO-TDA states in the CD and RD pathways for a water-ammonia dimer	Pg. S5
4. LE/LE and LE/CT electronic couplings for the $C_2H_4 - C_2F_4$ dimer	Pg. S6
5. uLE and orbital energies for the $C_2H_4 - C_2F_4$ dimer	Pg. S7
6. LE/LE and LE/CT electronic couplings for the adenine-thymine dimer	Pg. S8
7. Orbital energies for the adenine-thymine dimer	Pg. S9
8. Effect of truncating the virtual space on the uLE and uCT energies and electronic couplings of the chlorophyll dimer	Pg. S10

# 1. Effect of truncating the virtual space on the uLE energies of the isolated $C_2H_4 - C_2F_4$ and adenine-thymine dimers

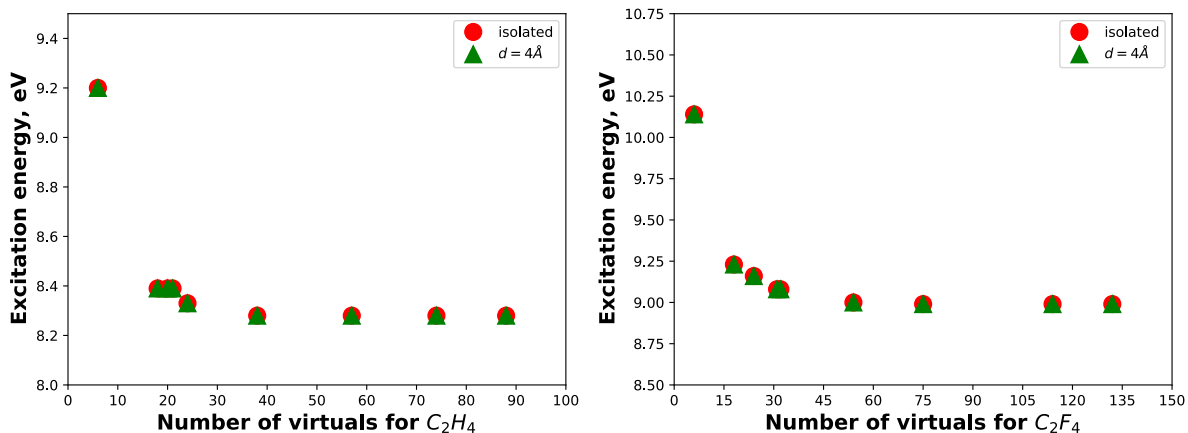


Figure S1: Effect of truncation of the number of virtual orbitals on the  $uLE_1$  (left panel) and  $uLE_2$  (right panel) excitation energies for the isolated fragments and the  $C_2H_4 - C_2F_4$  dimer at  $d = 4 \text{ \AA}$ .

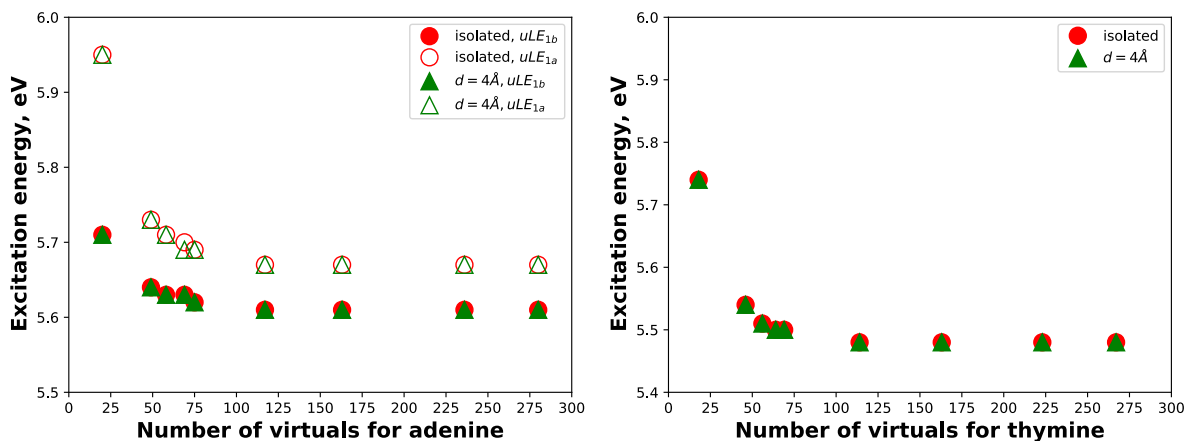


Figure S2: Effect of truncation of the number of virtual orbitals on the  $uLE_{1a}$ ,  $uLE_{1b}$  (left panel) and  $uLE_2$  (right panel) excitation energies for the isolated fragments and the adenine-thymine dimer at  $d = 4 \text{ \AA}$ .

## 2. Effect of truncating the virtual space on electronic couplings of the $C_2H_4 - C_2F_4$ and adenine-thymine dimers

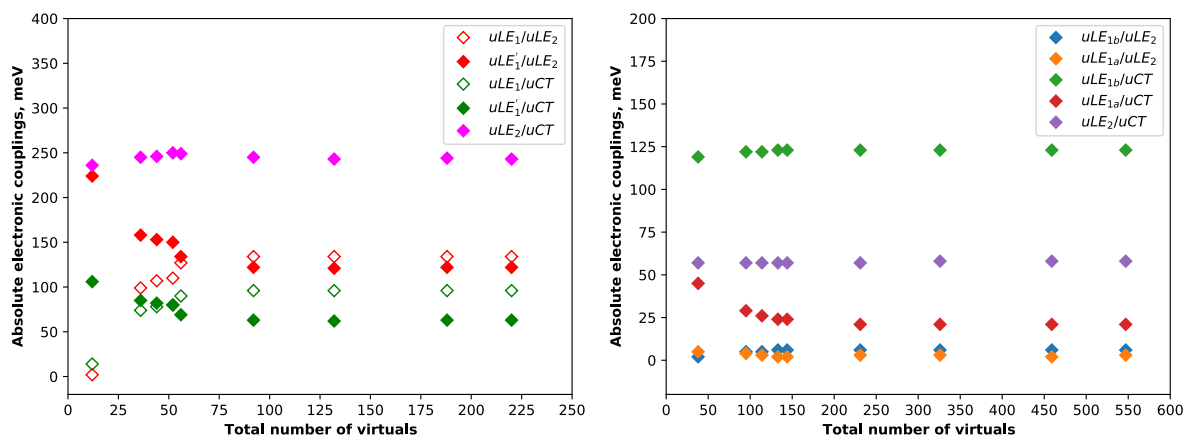


Figure S3: Absolute electronic couplings between the uLE and uCT states of the  $C_2H_4 - C_2F_4$  (left panel) and adenine-thymine (right panel) dimers with respect to the number of hard virtual orbitals used in the localization procedure, using the RILMO-TDA method.

### 3. Convergence of the RILMO-TDA states in the CD and RD pathways for a water-ammonia dimer

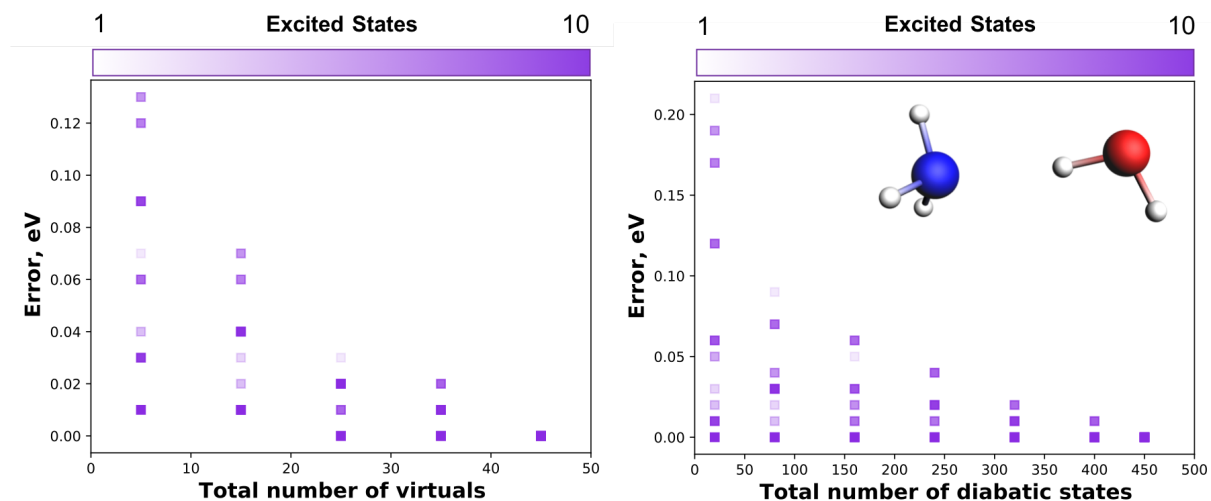


Figure S4: Left panel: Error in excitation energy (as compared to the supermolecular CMO reference energies) due to RILMO truncation of hard virtual orbitals for the lowest 10 RILMO-TDA (CD) states. Right panel: Error in excitation energy (as compared to the supermolecular CMO reference energies) due to truncation to  $M$  diabatic states for the lowest 10 RILMO-TDA (RD, $M$ ) states, while keeping all the hard virtual orbitals in the localization procedure. Calculations were carried out at CAMB3LYP/DZP level of theory.

#### 4. LE/LE and LE/CT electronic couplings for the $C_2H_4 - C_2F_4$ dimer

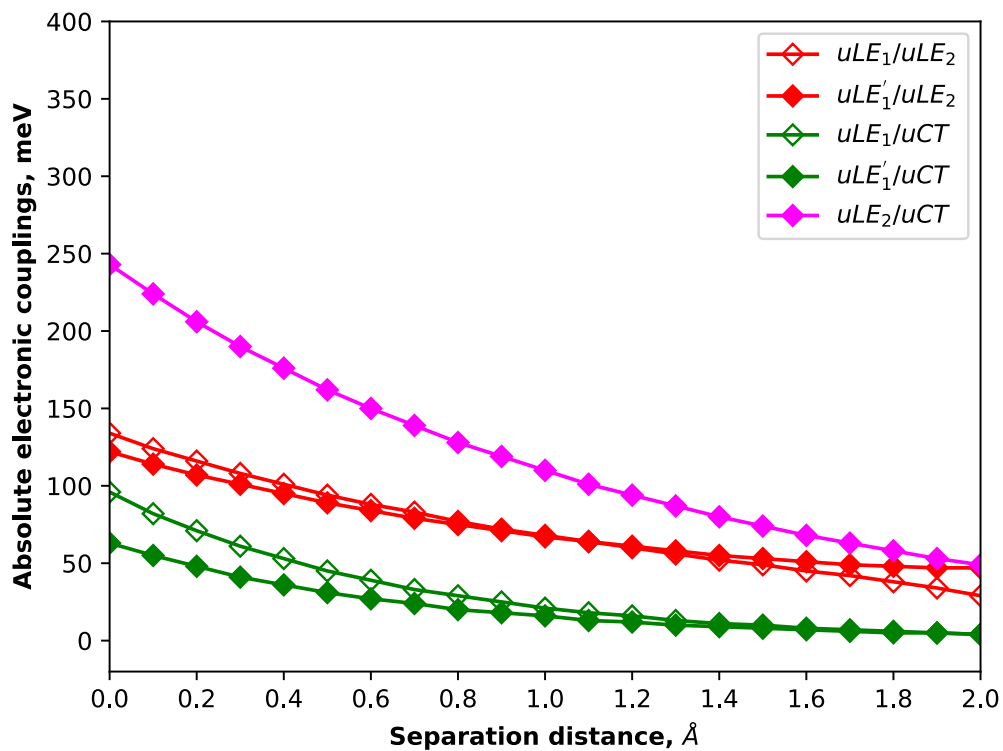


Figure S5: Absolute electronic couplings between the uLE and uCT states of the  $C_2H_4 - C_2F_4$  dimer with respect to the separation distance, using the RILMO-TDA method.

## 5. uLE and orbital energies for the $C_2H_4 - C_2F_4$ dimer

Table S1: uLE energies of the  $C_2H_4 - C_2F_4$  dimer using RILMO-TDA and PbE-sTDA methods at varying distances,  $d$  (Å). All units are in eV.

		$d = 0$	$d = 0.5$	$d = 1.0$	$d = 1.5$	$d = 2.0$
<b>RILMO-TDA</b>	<b>uLE<sub>1</sub></b>	8.33	8.31	8.30	8.29	8.28
	<b>uLE'<sub>1</sub></b>	8.55	8.44	8.36	8.32	8.29
	<b>uLE<sub>2</sub></b>	9.03	9.02	9.00	9.00	8.99

Table S2: Orbital energies associated with the uLE and uCT transitions of the  $C_2H_4 - C_2F_4$  dimer obtained from RILMO and PbE-sDFT methods at varying distances  $d$  (Å). Also shown are the isolated fragment energies. The uCT and uLE states in the main text comprises of : 1)  $uLE_1 : HOMO(1) \rightarrow LUMO(1)$ , 2)  $uLE_2 : HOMO(2) \rightarrow LUMO(2)/LUMO + 1(2)$  and 3)  $uCT : HOMO(2) \rightarrow LUMO(1)$ . (1) and (2) refer to fragments  $C_2H_4$  and  $C_2F_4$  respectively. All units are in eV.

		$d = 0$	$d = 0.5$	$d = 1.0$	$d = 1.5$	$d = 2.0$	isolated
<b>RILMO</b>	<b>LUMO(1)</b>	1.05	1.07	1.08	1.09	1.10	1.14
	<b>LUMO + 1(2)</b>	1.69	1.65	1.63	1.61	1.60	1.56
	<b>HOMO(1)</b>	-9.42	-9.37	-9.34	-9.32	-9.31	-9.27
	<b>HOMO(2)</b>	-9.15	-9.18	-9.20	-9.22	-9.23	-9.27
<b>PbE-sDFT</b>	<b>LUMO(1)</b>	1.26	1.22	1.19	1.19	1.19	1.23
	<b>LUMO(2)</b>	1.84	1.80	1.76	1.74	1.72	1.68
	<b>HOMO(1)</b>	-9.37	-9.33	-9.31	-9.29	-9.28	-9.24
	<b>HOMO(2)</b>	-9.04	-9.07	-9.09	-9.11	-9.12	-9.16

## 6. LE/LE and LE/CT electronic couplings for the adenine-thymine dimer

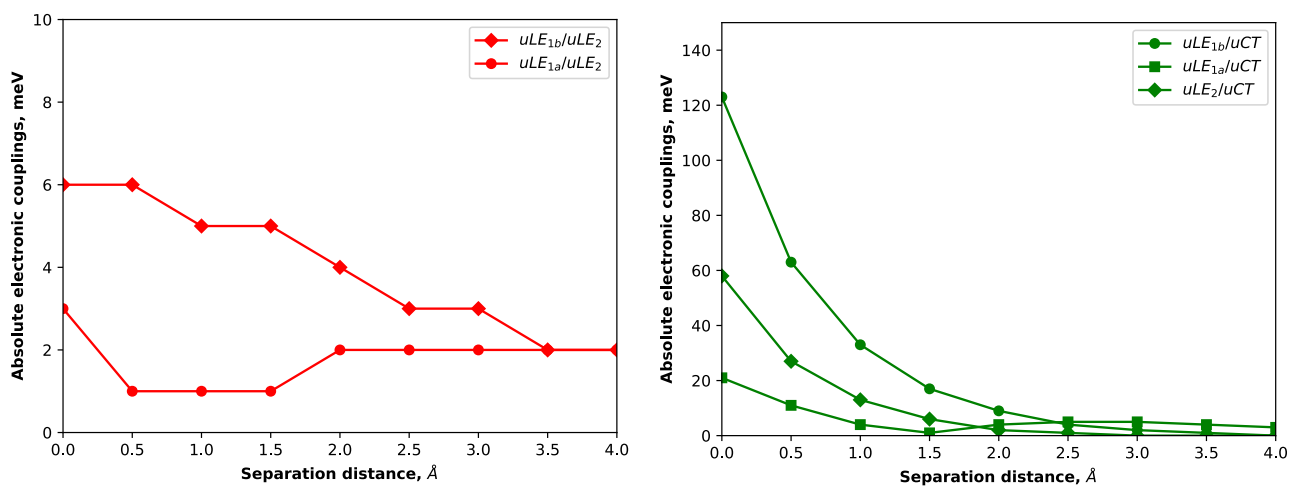


Figure S6: Absolute electronic couplings between the uLE/uLE states (left panel) and the uLE/uCT states (right panel) of the adenine-thymine dimer with respect to the separation distance, using the RILMO-TDA method.

## 7. Orbital energies for the adenine-thymine dimer

Table S3: Orbital energies associated with the uLE and uCT transitions of adenine-thymine dimer obtained from RILMO and PbE-sDFT methods at varying distances  $d$  (Å). Also shown are the isolated fragment energies. The uCT and uLE states in the main text comprises of : 1)  $uLE_{1a} : HOMO(1) \rightarrow LUMO(1)$ , 2)  $uLE_{1b} : HOMO(1) \rightarrow LUMO+1(1)/LUMO+2(1)$  , 3)  $uLE_2 : HOMO(2) \rightarrow LUMO(2)$  and  $uCT : HOMO(1) \rightarrow LUMO(2)$  . (1) and (2) refer to fragments adenine and thymine respectively. All orbital energies are in eV.

		$d = 0$	$d = 1.0$	$d = 2.0$	$d = 3.0$	$d = 4.0$	isolated
<b>RILMO</b>	<b>LUMO + 1(1)/LUMO + 2(1)</b>	1.17	1.14	1.16	1.16	1.15	1.14
	<b>LUMO(1)</b>	0.39	0.36	0.35	0.34	0.33	0.33
	<b>LUMO(2)</b>	-0.23	-0.28	-0.31	-0.32	-0.33	-0.36
	<b>HOMO(1)</b>	-7.72	-7.72	-7.73	-7.74	-7.74	-7.75
	<b>HOMO(2)</b>	-8.36	-8.39	-8.40	-8.42	-8.43	-8.46
<b>PbE-sDFT</b>	<b>LUMO + 1(1)</b>	1.40	1.32	1.30	1.30	1.29	1.28
	<b>LUMO(1)</b>	0.59	0.51	0.50	0.48	0.48	0.47
	<b>LUMO(2)</b>	-0.04	-0.15	-0.19	-0.20	-0.21	-0.25
	<b>HOMO(1)</b>	-7.60	-7.60	-7.60	-7.61	-7.61	-7.63
	<b>HOMO(2)</b>	-8.26	-8.29	-8.32	-8.33	-8.34	-8.38

## 8. Effect of truncating the virtual space on the uLE and uCT energies and electronic couplings of the chlorophyll dimer

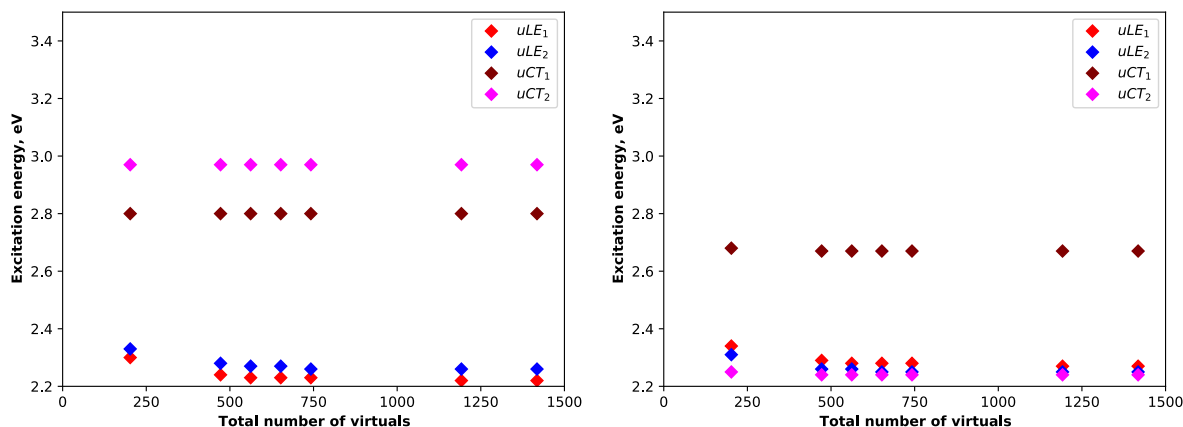


Figure S7: Excitation energies of the uLE and uCT states of conformation 1 (left panel) and conformation 2 (right panel) with respect to the number of hard virtual orbitals used in the localization procedure, using the RILMO-TDA method.

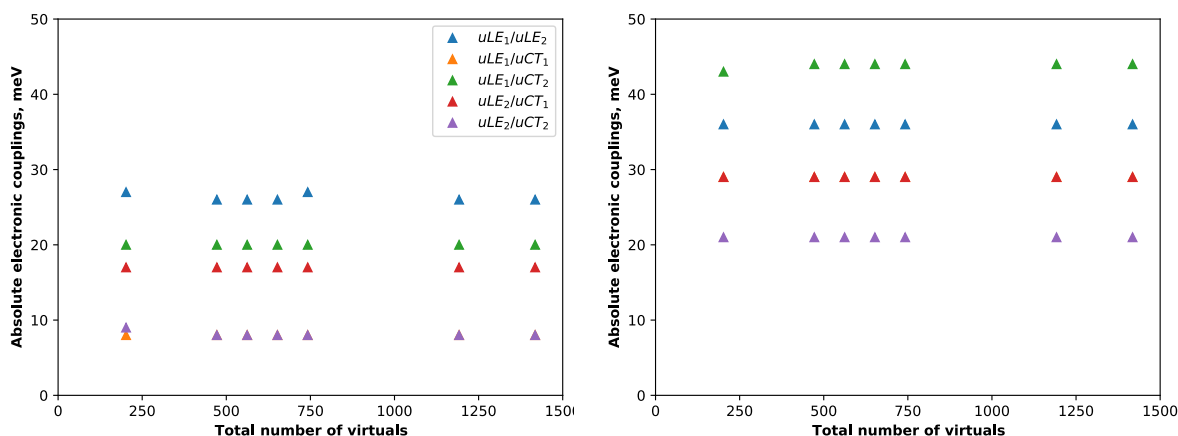


Figure S8: Absolute electronic couplings between the uLE and uCT states of conformation 1 (left panel) and conformation 2 (right panel) with respect to the number of hard virtual orbitals used in the localization procedure, using the RILMO-TDA method.